RSC Medicinal Chemistry

ROYAL SOCIETY OF CHEMISTRY

RESEARCH ARTICLE

View Article Online
View Journal | View Issue

Open Access Article. Published on 09 October 2024. Downloaded on 10/27/2025 5:03:29 PM.
This article is licensed under a Creative Commons Attribution-NonCommercial 3.0 Unported Licence.

Check for updates

Cite this: *RSC Med. Chem.*, 2025, **16**, 346

Azo derivatives of monoterpenes as anti-*Helicobacter pylori* agents: from synthesis to structure-based target investigation†

Francesco Melfi,‡[a] Marialuigia Fantacuzzi,‡[a] Simone Carradori,*[a] Ilaria D'Agostino,[b] Alessandra Ammazzalorso,[a] Noemi Mencarelli,[a] Marialucia Gallorini,[a] Mattia Spano,[c] Paolo Guglielmi,[c] Mariangela Agamennone,[a] Sazan Haji Ali,[de] Ali Al-Samydai[f] and Francesca Sisto[g]

Received 7th July 2024,
Accepted 7th October 2024

DOI: 10.1039/d4md00511b

rsc.li/medchem

Helicobacter pylori (*Hp*) infection affects nearly half of the global population. Current therapeutic options include the administration of a combination of antibiotics and proton pump inhibitors, although antimicrobial resistance rise remains a big concern. Phenolic monoterpenes, *e.g.*, eugenol, vanillin, carvacrol, and thymol, have always attracted researchers for their multifaced biological activities and the possibility to be easily derivatized. Thereby, herein we present the functionalization of such compounds through the conventional aryl diazotization reaction, generating a series of mono- and bis-azo derivatives (**1–28**). Also, to continue previous studies, we investigated the role of the free phenolic moiety of thymol with eight compounds (**29–36**). The compounds were tested against four *Hp* strains including three clinical isolates, finding some potent and selective inhibitors of bacterial growth. Thus, the representative compounds underwent *in vitro* cytotoxicity evaluation on two normal cell lines and putative target investigation by performing a structure-based approach based on docking calculations on some of the most studied pharmacological targets for *Hp*, *e.g.*, urease, β-hydroxyacyl-acyl carrier protein dehydratase, glucose 6-phosphate dehydrogenase, and inosine 5′-monophosphate dehydrogenase.

1. Introduction

Helicobacter pylori (*Hp*) is a microaerophilic, Gram-negative, spiral-shaped bacterium infecting an estimated 50% of the global population.[1] The prevalence of this infection is influenced by different factors related to geographic regions, hygiene conditions, temperature, and socioeconomic status.[2] Recently, a meta-analysis estimated the overall prevalence of *Hp* infection worldwide, highlighting a downward trend in adults in the past three decades (52.6% before 1990, 43.9% from 2015 to 2022), and an upward fashion for children and adolescents (from 26.6% before 1990 to 35.1% from 2015 to 2022).[3] *Hp* colonizes the inhospitable gastric environment by several mechanisms including urease activity, motility, and adhesion.[4] Even though the infection is usually asymptomatic, it is correlated with a series of diseases, including duodenal and gastric ulcers, and malignancies such as mucosa-associated lymphoid tissue (MALT) lymphoma and gastric cancer.[1] As a matter of fact, the International Agency for Research on Cancer (IARC), a subordinate organization of the World Health Organization (WHO), classified *Hp* as a group 1 carcinogen.[5] Currently, the eradication of the infection relies on treatments including the combination of antibiotics and strong acid suppressants.[4] In particular, the first-line treatment is based on a triple therapy including proton pump inhibitors (PPIs), clarithromycin, and amoxicillin. However, if the treatment population has a clarithromycin resistance rate above 20%, clarithromycin-containing triple therapy is not indicated. Thus, bismuth-containing quadruple therapy (BQT) or non-bismuth

[a] *Department of Pharmacy, "G. d'Annunzio" University of Chieti-Pescara, via dei Vestini 31, 66100 Chieti, Italy. E-mail: simone.carradori@unich.it*
[b] *Department of Pharmacy, Univerity of Pisa, Via Bonanno 6, 56126 Pisa, Italy*
[c] *Department of Drug Chemistry and Technology, "Sapienza" University of Rome, P. le Aldo Moro 5, 00185 Rome, Italy*
[d] *Department of Pharmaceutical Chemistry, College of Pharmacy, Hawler Medical University, Erbil 44000, Iraq*
[e] *Department of Pharmaceutical Chemistry, Faculty of Pharmacy, Anadolu University, Eskişehir, 26470, Turkey*
[f] *Pharmacological and Diagnostic Research Centre (PDRC), Faculty of Pharmacy, Al-Ahliyya Amman University, Amman-Jordan- Al Salt Road, Amman, 19328, Jordan*
[g] *Department of Biomedical, Surgical and Dental Sciences, University of Milan, Via Pascal 36, 20133 Milan, Italy*

† Electronic supplementary information (ESI) available: The supplementary material file contains the NMR spectra of the compounds reported in this article. See DOI: https://doi.org/10.1039/d4md00511b

‡ These authors contributed equally to the work.

 This journal is © The Royal Society of Chemistry 2025

Open Access Article. Published on 09 October 2024. Downloaded on 10/27/2025 5:03:29 PM.
This article is licensed under a Creative Commons Attribution-NonCommercial 3.0 Unported Licence.

quadruple therapy could be -used as a first line empirical treatment.[4] Albeit a seven-day first-line treatment usually leads to eradication rates exceeding 90%, antibiotic resistance insurgence, insufficient acid suppression, and inadequate adherence to medications, can cause alarming failures,[6–8] drawing attention to the importance of developing novel and effective anti-*Hp* therapies.[9] However, only a few new antibiotics have received approval for the market in the past years and the search for new chemical entities is urgently required.[10–13]

In recent years azo benzene compounds have been extensively explored given their broad spectrum of pharmaceutical and industrial applications and their cost-effective, easy, and highly reproducible synthetic procedure. Notably, azo derivatives from substituted anilines resulted in the development of derivatives endowed with a versatile biological profile, including antimicrobial activity.[14–16]

Conversely, to date, only a few researchers investigated the azo compounds as effective tools for the management of *Hp* and, among them, Jangra and colleagues reported a series of substituted 3-aryldiazenyl indoles targeting the *Hp* inosine 5′-monophosphate dehydrogenase (IMPDH, EC 1.1.1.205) enzyme.[17] Furthermore, azobenzene derivatives can be degraded by intestinal microorganisms *in vivo*, as demonstrated by Chung *et al.*, leading to carcinogenic and/or toxic metabolites, after azo-reduction by intestinal anaerobes.[18] On the other hand, the wide polypharmacology of monoterpenes led to an in-depth investigation of carvacrol (**Car**, Fig. 1) and thymol (**Thy**, Fig. 1) along with eugenol (**Eu**, Fig. 1) and vanillin (**Van**, Fig. 1) and their regioisomers *o*-eugenol (***o*-Eu**, Fig. 1), iso-eugenol (**iso-Eu**, Fig. 1), and *o*-vanillin (***o*-Van**, Fig. 1) as antimicrobials. In this context, we recently reported the ability of **Thy**-, **Eu**-, and **Car**-based compounds to act as inhibitors of *Hp* growth.[19–21]

Also, by combining the two chemical features, Prof. Kantar's research group evaluated a series of azo compounds containing a **Eu**, **Van**, and guaiacol (**Gu**, Fig. 1) core, demonstrating promising inhibitory activity against *Hp* urease and antibacterial effectiveness.[22–25]

Pursuing our efforts in the development of novel effective anti-*Hp* drugs and inspired by the antimicrobial results observed for azo compounds, we designed a series of novel azobenzene derivatives based on the phenolic monoterpenes **Thy**, **Car**, **Eu**, and **Van**. The derivatives were synthesized through the conventional diazotization-coupling reaction, as depicted in Scheme 1. The antibacterial activity for these compounds along with a panel of commercially available phenolic monoterpenes and derivatives was assessed against *Hp* strains, including the genomically characterized NCTC 11637 and three other clinical isolates (F1, 23, and F4), and reported as minimal inhibitory concentration (MIC) and minimal bactericidal concentration (MBC). Finally, two of the most active compounds (**20** and **28**) have been tested on healthy cell lines to assess their safety and subjected to a target investigation protocol by means of a molecular docking protocol employing a reverse docking approach to unravel the putative target(s) among the most extensively studied, including urease (urea amidohydrolase, EC 3.5.1.5), β-hydroxyacyl-acyl carrier protein (ACP) dehydratase (FabZ, EC 4.2.1.59), glucose 6-phosphate dehydrogenase (G6PD, EC 1.1.1.49), and inosine 5′-monophosphate dehydrogenase (IMPDH).

2. Results and discussion

2.1. Design and synthesis of the monoterpene derivatives

A new series of azobenzene derivatives (**1–36**) was obtained through the conventional diazotization-coupling reaction by using the appropriately substituted aromatic amine (**A**, Scheme 1) under acidic conditions in the presence of sodium nitrite at 0 °C, followed by the addition of the appropriate phenolic monoterpene in a basic environment (Scheme 1).

Starting from **Eu** and **Van**, one azo compound (**B**, Scheme 1) was obtained, while interestingly, despite using the same experimental procedure involving equimolar amounts of the starting materials, in several cases, two products (**C** and **E**, Scheme 1) were isolated when **Car** and **Thy** were employed. In particular, the expected derivative characterized by the azo function at *para*-position to the phenolic OH moiety (**C**) was obtained as the major product, while the bis-azo compound **E** endowed with two azo

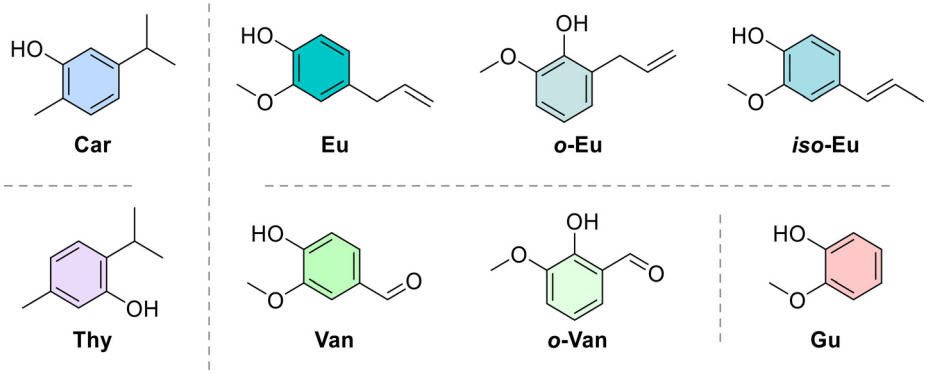

Fig. 1 Chemical structures of natural monoterpenes and their derivatives.

Open Access Article. Published on 09 October 2024. Downloaded on 10/27/2025 5:03:29 PM.
This article is licensed under a Creative Commons Attribution-NonCommercial 3.0 Unported Licence.

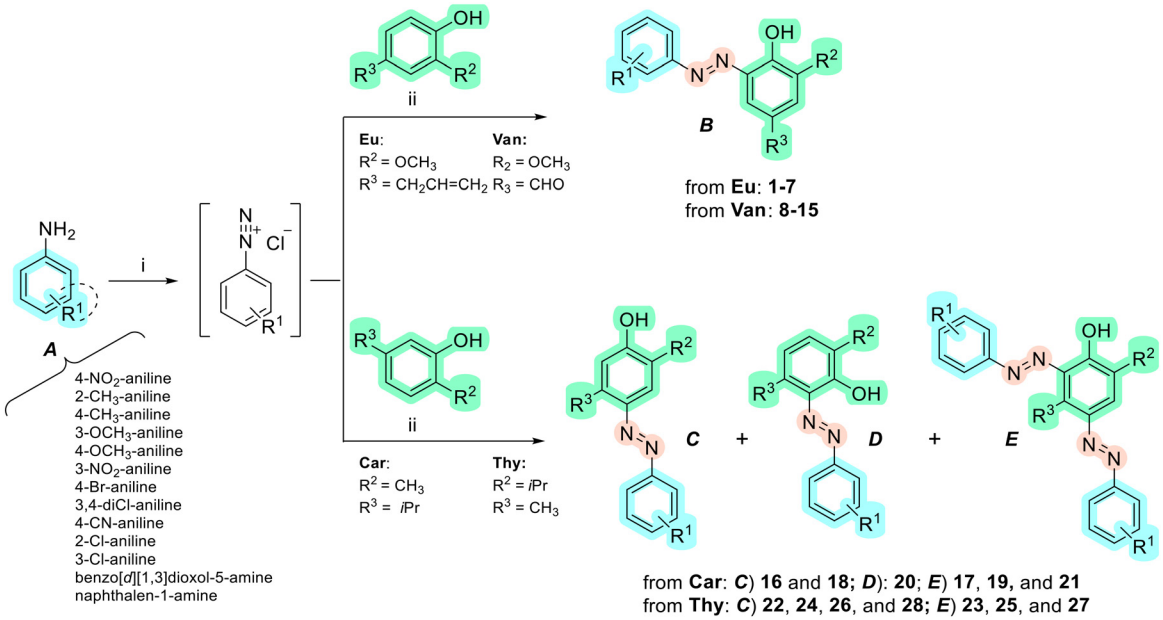

Scheme 1 Synthetic routes to azo compounds **1**–**36**. Reagents and conditions: (i) $NaNO_2$, 1.2 M HCl, 0 °C, 5 min; (ii) substituted phenol, 1.3 M NaOH, 0 °C, 5 min.

functions at both *ortho* and *para* positions with respect to the phenolic group was isolated only in low yields. Moreover, only in one case, when **Car** was coupled with 4-nitroaniline (**20**), were we able to isolate only the *ortho*-azo product (**D**).

Then, with the aim to better understand the role of phenolic function in the anti-*Hp* activity, this function was chemically modified through *O*-derivatization reactions on two compounds (**26** and **28**, characterized by an electron-withdrawing or an electron-donating moiety, respectively), including methylation (**29**, **33**), acetylation (**30**, **34**), and conversion into dimethyl(thio)carbamates (**31**, **32**, **35**, **36**) (Scheme 2).

O-Methylation of **26** and **28** was performed through an excess of dimethyl sulfate in the presence of K_2CO_3 at room temperature (r.t.) to afford the methoxy derivatives **29** and **33**, respectively. Then, by singularly reacting **26** and **28** with sodium bicarbonate ($NaHCO_3$) and an excess of acetic anhydride (Ac_2O) at r.t., acetylated **30** and **34** were easily obtained. In the end, compounds **31**, **32**, **35**, and **36** were obtained by reacting the suitable **26** or **28** with dimethyl (thio)carbamoyl chloride and potassium carbonate (K_2CO_3) as a base at r.t.

Interestingly, for all these compounds, the N═N double bond was found to be totally in the *E* configuration. In fact, the ^{1}H NMR spectra showed the presence of just one species

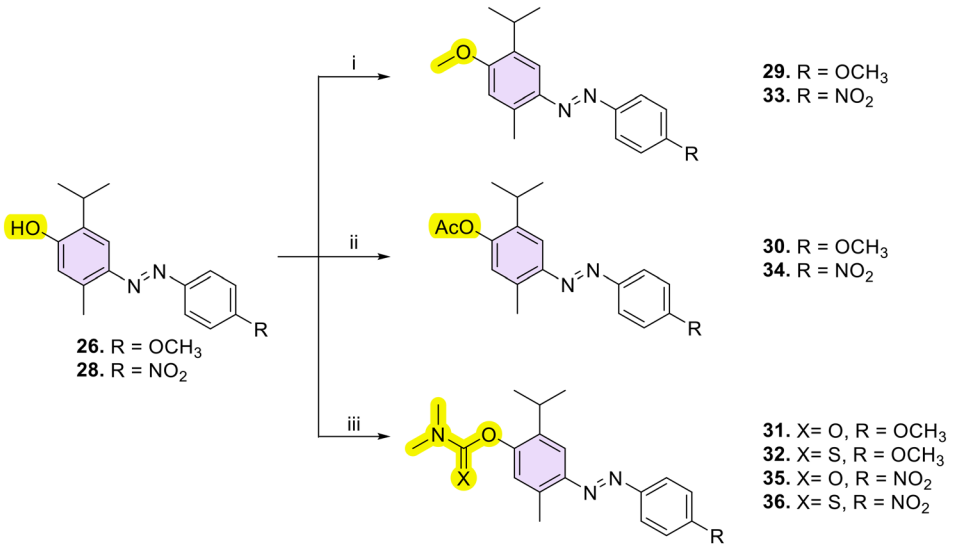

Scheme 2 Synthetic routes to *O*-derivatized compounds **29**–**36**. Reagents and conditions: (i) K_2CO_3, dimethylsulfate, r.t., 24 h; (ii) $NaHCO_3$, Ac_2O, r.t., 24 h; (iii) dimethyl (thio)carbamoyl chloride, K_2CO_3, ACN, r.t., 24 h.

Open Access Article. Published on 09 October 2024. Downloaded on 10/27/2025 5:03:29 PM.
This article is licensed under a Creative Commons Attribution-NonCommercial 3.0 Unported Licence.

(ESI†), then confirmed to be the *E* isomer, as previously established by UV-vis experiments.[26]

2.2. *In vitro* antibacterial activity evaluation against *H. pylori* and other bacterial species

The antibacterial profile of the commercial monoterpenes and their analogues, and the synthesized azo derivatives **1–36**, was assessed on four *Hp* strains, including the reference NCTC 11637 strain and the clinical isolates F1, 23, and F4 from our laboratory by using metronidazole (**MTZ**), clarithromycin (**CLR**), and amoxicillin (**AMX**) as reference antibiotics (Table 1).

The phenotypic diversity of resistant strains influences the biological results of both parent compounds and their derivatives. Indeed, this depends on the genotypic differences among resistant and sensitive strains. It is also known that the **CLR** resistance (F1 and F4) could be related to the mutation of the macrolide target, while the resistance to **MTZ** (like in NCTC 11637 and F4 strains) should be linked to the inactivation by mutation of the gene encoding an oxygen-independent NADPH nitroreductase.[21]

By analyzing the anti-*Hp* activities of the parent phenolic monoterpenes, we noticed that only ***o*-Van**, characterized by methoxy and aldehyde groups at the *ortho* position of the hydroxy group, and iso-Eu, bearing the methoxy and prop-1-en-1-yl moieties, at the *ortho* and *para* positions of the phenolic function, exhibited a promising antibacterial activity (Table 1). In particular, ***o*-Van** displayed a value between 4 and 16 μg mL^{-1} for both MIC and MBC, while **iso-Eu** reached a value of 32 μg mL^{-1} for MIC and MBC against all the tested strains. The other monoterpenes and analogues, including thymol blue, resulted in being almost or completely inactive on the four tested *Hp* strains (Table 1). In contrast, their azo analogues showed in some cases an anti-*Hp* activity with an MBC value of 2 μg mL^{-1}, especially for **Thy** and **Car** azo derivatives (Table 1).

Eu derivatives **1–7** resulted in being inactive on the four strains, mainly exhibiting MIC and MBC values of around 128 μg mL^{-1}, with the lipophilic/hydrophilic and electronic nature of substituents not affecting the activity profile (Table 1). Indeed, the most active compounds **4**, bearing a *para*-nitro substituent, and **2**, endowed with an *ortho*-methyl group, showed only in some cases MICs and MBCs of 64 μg mL^{-1} (Table 1).

Similarly, previously reported derivatives endowed with electron-donating substituents, *i.e.*, *para*-methyl or *para*-methoxy groups, showed higher activity on the NCTC 11637 strain, with MIC values of 64 and 32 μg mL^{-1}, respectively.[21] Otherwise, electron-withdrawing substituents, *i.e.*, *para*-cyano, *para*-bromo, and 3,4-dichloro substituents, were found to be almost inactive, with MIC values ≥128 μg mL^{-1}.[21] Interestingly, monochloro derivatives, with the halogen at the *meta* or *ortho* position, still remain the best-in-class **Eu** compounds, with MIC equal to 8–16 μg mL^{-1} on the tested strains.[21]

For **Van** derivatives **8–15**, a linear trend for the biological results was not highlighted, even though the introduction of a substituted phenyl ring through the azo function generally ameliorated the anti-*Hp* profile of the monoterpene (Table 1). In detail, the insertion of the bromine at the *para* position as in **13** led to an increase of the activity (MIC range: 8–32 μg mL^{-1}) especially on the F1 strain, while either its substitution with the other halogen, as for the 3-chlorine **9**, or the presence of two chlorine atoms at the *meta* and *para* positions (**15**) decreased dramatically the activity against all the strains. Otherwise, single chlorine at the *ortho* position (**8**) was a better option for chloro-derivatives, especially against the F1 strain, with MIC and MBC values of 16 μg mL^{-1}. Other electron-withdrawing groups like the cyano substituent placed at the *para* (**14**) or the nitro moiety at the *meta* position (**10**) showed better results with MBC values of 4 to 16 μg mL^{-1}, respectively. The presence of electron-donating substituents in *para* led to different results depending on the magnitude of the electron-releasing effect. As a matter of fact, compound **12**, endowed with a stronger electron-donating methoxy group, exhibited a weak or null activity, while compound **11**, with the weaker methyl group, resulted to be the most potent **Van** derivative with both MIC and MBC values in the range of 2–8 μg mL^{-1}, showing more efficacy against the F1 strain (Table 1).

Car and **Thy** derivatives (**16–21** and **22–28**, respectively) showed different trends: on the one hand, the mono-azo derivatives resulted to be the most potent ones against *Hp* overall, while the molecules that presented two azo functions in their structure, the bis-azo derivatives **17**, **19**, **21**, **23**, **25**, and **27**, were completely inactive, suggesting that an enlargement of the scaffold could lead to excessive bulkiness or lipophilicity, decreasing the antibacterial potency (Table 1). In terms of activity, there was only a slight difference between the *para*-methoxy **Car**-based compound **18** and its **Thy**-based regioisomer **26**, with the former exhibiting MICs between 4 and 8 μg mL^{-1}, whereas the latter showed better outcomes (2–4 μg mL^{-1}) and also exhibiting a potent activity on the F4 strain (2 μg mL^{-1}). Moreover, derivatives **16** and **24**, the *ortho*-chloro azo derivatives of **Car** and **Thy**, respectively, showed a similar inhibitory profile, with the only exception of MIC and MBC values for F4 (2 μg mL^{-1}) for compound **16** instead of 4 μg mL^{-1} as observed for **24**. The *para*-methyl substituted azo derivative of **Thy** (**22**) exhibited 4 μg mL^{-1} for MIC and MBC on all the clinical isolates. Lastly, *para*-nitro derivatives **20** and **28** showed the best inhibitory profile on most strains: both compounds exhibited MIC and MBC values on F1, 23, and NCTC 11637 equal to 2 μg mL^{-1}, while in the case of the F4 strain, the values were equal to 4 μg mL^{-1}. Moreover, **20** resulted in strongly inhibiting the growth of strains 23 and NCTC 11637, while **28** was found to be active against the F1 strain (Table 1).

It is interesting to note that when the phenolic group of compounds **26** and **28** was derivatized as in **29–32** and **33–36**, respectively, a dramatic decrease of activity independently of the chemical characteristics of the derivatization occurred

Open Access Article. Published on 09 October 2024. Downloaded on 10/27/2025 5:03:29 PM.
This article is licensed under a Creative Commons Attribution-NonCommercial 3.0 Unported Licence.

Table 1 Anti-*Hp* activity (MIC and MBC values) of commercial monoterpenes and derivatives, newly synthesized azo compounds **1**–**36**, and reference antibiotics

Compound		Structure	MIC/MBC (μg mL^{-1}) on *H. pylori* strains				MIC_{50}/MIC_{90} (μg mL^{-1})	MBC_{90} (μg mL^{-1})
			F1	**23**	NCTC 11637	F4		
Commercially available	**Eu**	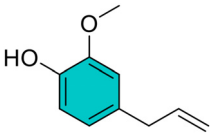	64/128	64/64	32/64	64/64	64/64	128
	***o*-Eu**	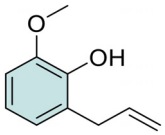	>128/>128	>128/>128	>128/>128	>128/>128	>128/>128	>128
	iso-Eu	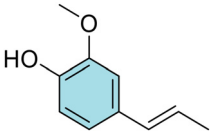	32/32	32/32	32/32	32/32	32/32	32
	Van	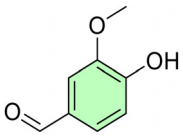	>128/>128	>128/>128	>128/>128	128/128	>128/>128	>128
	***o*-Van**	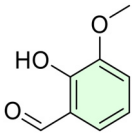	4/4	16/16	8/16	8/8	8/16	16
	Car	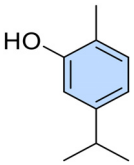	64/64	64/64	64/64	64/64	64/64	64
	Thy	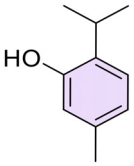	64/64	128/128	128/128	64/64	64/128	128
	Thymol blue	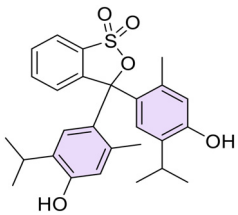	128/128	128/>128	>128/>128	>128 >128	128/>128	>128
Eu azo derivatives	**1**	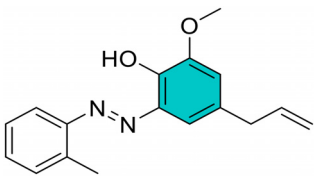	128/128	64/64	128/128	64/64	64/128	128
	2	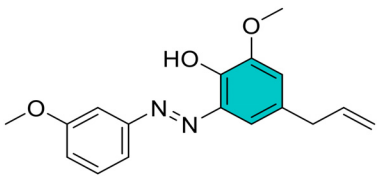	128/>128	>128/>128	128/>128	>128/>128	128/>128	>128

Open Access Article. Published on 09 October 2024. Downloaded on 10/27/2025 5:03:29 PM.
This article is licensed under a Creative Commons Attribution-NonCommercial 3.0 Unported Licence.

Table 1 *(continued)*

Compound		Structure	MIC/MBC (μg mL^{-1}) on *H. pylori* strains				MIC_{50}/MIC_{90} (μg mL^{-1})	MBC_{90} (μg mL^{-1})
			F1	**23**	NCTC 11637	F4		
	3	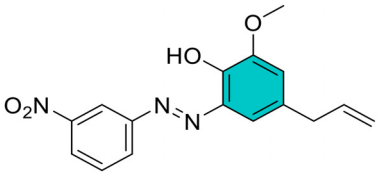	128 />128	128/128	128/128	128/128	128/>128	>128
	4	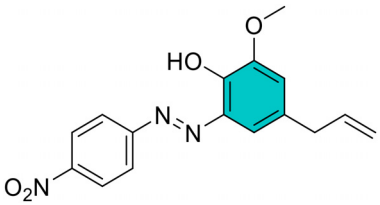	64/64	128/128	64/64	64/128	64/128	128
	5	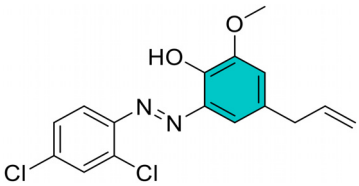	>128/>128	>128/>128	128/128	>128/>128	>128/>128	>128
	6	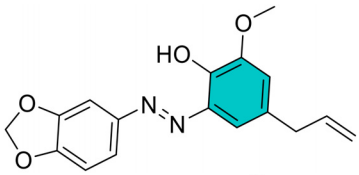	>128/>128	>128/>128	128/128	>128/>128	>128/>128	>128
	7	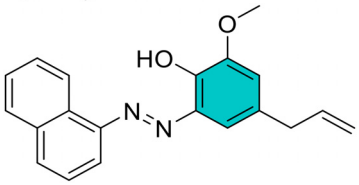	>128/>128	>128/>128	128/128	>128/>128	>128/>128	>128
Van azo derivatives	**8**	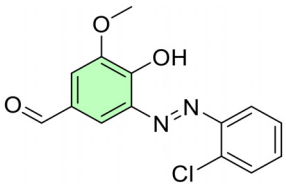	16/16	64/64	64/64	64/64	64/64	64
	9	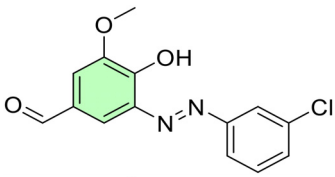	128/128	128/128	128/>128	128/128	128/>128	>128
	10	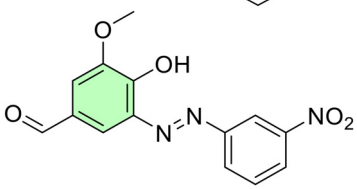	16/16	8/8	8/8	8/16	8/16	16
	11	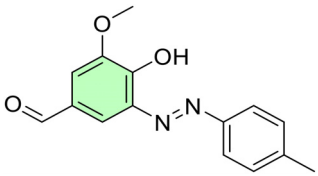	2/2	8/8	4/4	8/8	4/8	8

Open Access Article. Published on 09 October 2024. Downloaded on 10/27/2025 5:03:29 PM.
This article is licensed under a Creative Commons Attribution-NonCommercial 3.0 Unported Licence.

Table 1 *(continued)*

Compound		Structure	MIC/MBC (μg mL^{-1}) on *H. pylori* strains				MIC_{50}/MIC_{90} (μg mL^{-1})	MBC_{90} (μg mL^{-1})
			F1	**23**	NCTC 11637	F4		
	12	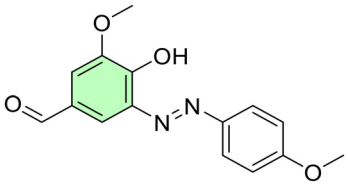	64/128	>128/>128	>128/>128	>128/>128	>128/>128	>128
	13	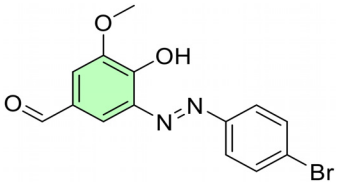	8/8	32/32	16/16	16/16	16/32	32
	14	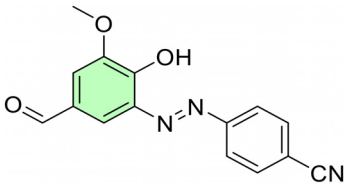	4/4	8/8	8/16	8/8	8/8	16
	15	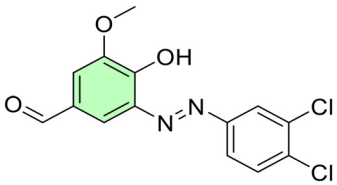	64 /64	64/128	128/128	128/128	64/128	128
Car azo derivatives	**16**	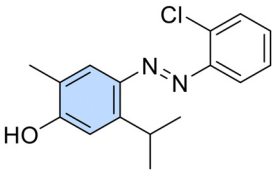	4/4	4/4	4/4	2/2	4/4	4
	17	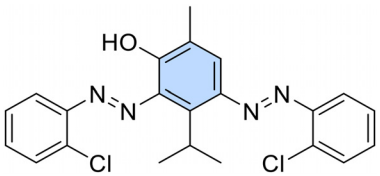	64/>128	128/>128	128/128	128/>128	128/128	>128
	18	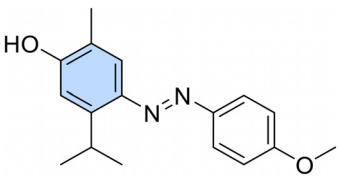	4/4	8/8	8/8	4/4	4/8	8
	19	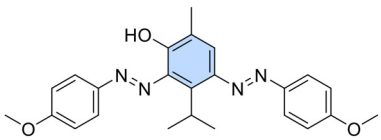	>128/>128	>128/>128	>128/>128	>128/>128	>128/>128	>128
	20	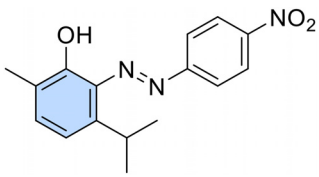	2/4	2/2	2/2	4/4	2/4	4

Open Access Article. Published on 09 October 2024. Downloaded on 10/27/2025 5:03:29 PM.
This article is licensed under a Creative Commons Attribution-NonCommercial 3.0 Unported Licence.

Table 1 *(continued)*

Compound		Structure	MIC/MBC (μg mL^{-1}) on *H. pylori* strains				MIC_{50}/MIC_{90} (μg mL^{-1})	MBC_{90} (μg mL^{-1})
			F1	**23**	NCTC 11637	F4		
	21	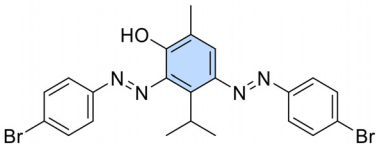	>128/>128	>128/>128	128/128	>128/>128	>128/>128	>128
Thy azo derivatives	**22**	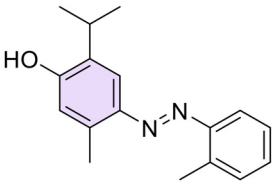	4/4	8/8	4/4	4/4	4/8	8
	23	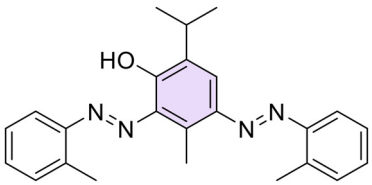	128/>128	128/>128	>128/>128	128/>128	128/>128	>128
	24	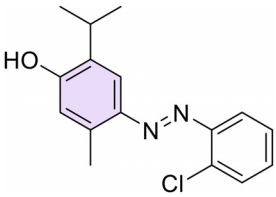	4/4	4/8	4/4	4/4	4/4	8
	25	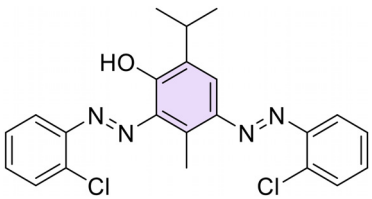	128/>128	128/>128	>128/>128	128/>128	128/>128	>128
	26	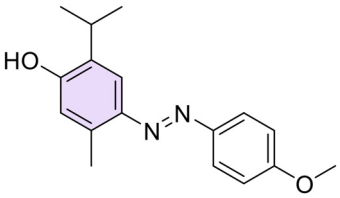	4/4	4/4	4/4	2/2	4/4	4
	27	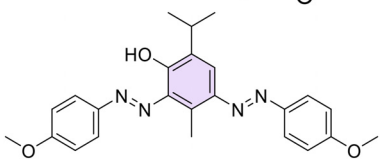	128/>128	128/>128	>128/>128	128/>128	128/>128	>128
	28	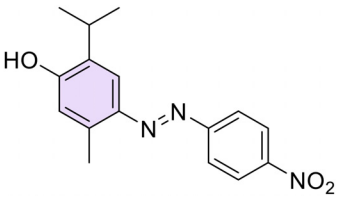	2/2	2/2	2/2	4/4	2/4	4
O-Modified derivatives of **26**	**29**	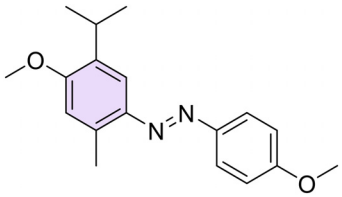	128/>128	>128/>128	>128/>128	128/128	128/>128	>128

Open Access Article. Published on 09 October 2024. Downloaded on 10/27/2025 5:03:29 PM.
This article is licensed under a Creative Commons Attribution-NonCommercial 3.0 Unported Licence.

Table 1 *(continued)*

Compound		Structure	MIC/MBC (μg mL^{-1}) on *H. pylori* strains				MIC_{50}/MIC_{90} (μg mL^{-1})	MBC_{90} (μg mL^{-1})
			F1	**23**	NCTC 11637	F4		
	30	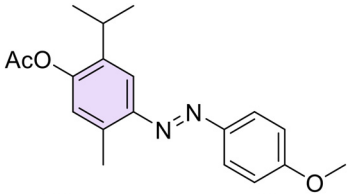	128/128	64/64	128/128	64/128	64/128	128
	31	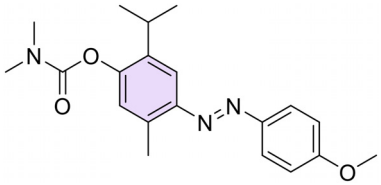	128/>128	64/128	64/128	64/64	64/128	>128
	32	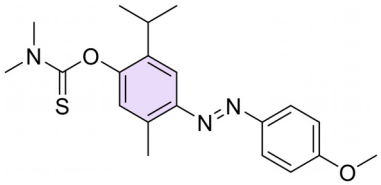	128/>128	128/128	>128/>128	128/128	128/>128	>128
O-Modified derivatives of **28**	**33**	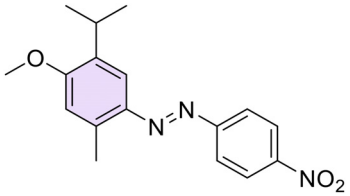	>128/>128	>128/>128	>128/>128	>128/>128	>128/>128	>128
	34	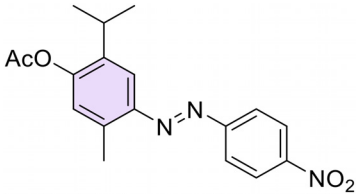	128/128	128/128	>128/>128	>128/>128	128/>128	>128
	35	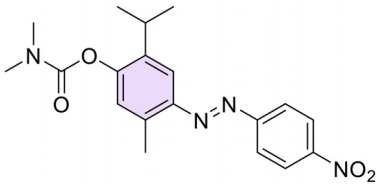	128/128	128/>128	128/>128	128/128	128/>128	>128
	36	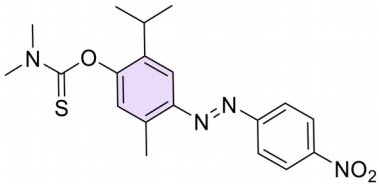	>128/>128	>128/>128	>128/>128	>128/>128	>128/>128	>128
Reference antibiotics	**MTZ**		2/2	1/1	256/256	32/32	2/256	256/256
	CLR		4/8	0.064/0.064	0.064/0.064	>256/>256	0.064/>256	>256/>256
	AMX		0.064/0.064	0.016/0.016	0.016/0.016	0.064/0.064	0.016/0.064	0.064
	Antibiotic susceptibility		**MTZ** **CLR+** **AMX−**	**MTZ−** **CLR−** **AMX−**	**MTZ+** **CLR−** **AMX−**	**MTZ+** **CLR+** **AMX−**		

MICs and MBCs are expressed in μg mL^{-1} as the average from experiments performed in triplicate. Antibiotic susceptibility was assessed according to the most recent EUCAST guidelines (Clinical Breakpoint Tables v. 14.0, valid from 1 January 2024). **MTZ+** = metronidazole resistant; **MTZ−** = metronidazole susceptible (MIC ≤8 μg mL^{-1}); **CLR+** = clarithromycin resistant; **CLR−** = clarithromycin susceptible (MIC ≤0.25 μg mL^{-1}); **AMX−** = amoxicillin susceptible (MIC ≤0.125 μg mL^{-1}).

Open Access Article. Published on 09 October 2024. Downloaded on 10/27/2025 5:03:29 PM.
This article is licensed under a Creative Commons Attribution-NonCommercial 3.0 Unported Licence.

(Table 1), suggesting that the free phenolic group is essential for the anti-*Hp* activity within this library of derivatives. This is in line with that observed for **Car**, **Thy**, and **Eu** *O*-functionalization with alkyl, alkenyl, acetyl, and ester groups previously explored.[19–21] Therefore, the chemically stable functionalization of the phenolic function is expected to increase the hydrophobicity of these compounds, and we could assume that the phenolic function of the azo derivatives influences the lipophilic/hydrophilic balance, affecting their antibacterial profile.

Furthermore, to shed light on the selectivity of the compounds' antibacterial effect, we tested the most potent anti-*Hp* derivatives **20** and **28** against three additional bacterial species: two Gram-negative, *e.g.*, the lactose-fermenting *Escherichia coli* ATCC 25922 and the non-lactose-fermenting *Pseudomonas aeruginosa* ATCC 27853, and the Gram-positive *Staphylococcus aureus* ATCC 29213, and MIC and MBC values are reported in Table 2.

By comparing data in Table 1, a lack of activity (MIC and MBC values >128 μg mL^{-1}) on the Gram-negative bacteria *E. coli* and *P. aeruginosa*, with a consequent high selectivity for *Hp* (MIC and MBC values in the range 2–4 μg mL^{-1}), was clear. Lower MIC values were obtained against the Gram-positive *S. aureus* (= 2 μg mL^{-1}), whereas worse MBC values (= 32 μg mL^{-1}) suggested a bacteriostatic effect for such compounds, as indicated by the MBC/MIC ratio greater than 4.

2.3. Molecular docking simulations

In the search for the pharmacological target of the azo derivatives and, in particular, of the two best-in-class compounds **20** and **28**, a ligand-based target fishing approach was performed. Briefly, we conducted an *in silico* reverse screening in which a query compound was compared to ligands of specific targets.[27,28] Different free web tools were used, like SwissTargetPrediction,[29] PLATO,[30] SuperPred,[31] PPB2,[32] and SEA Search.[33] However, in almost all databases no *Hp* or any other bacterial targets were included. Thus, a structure-based approach was employed. A series of docking simulations were conducted on the most extensively studied targets associated with *Hp*, namely urease, FabZ, G6PD, and IMPDH.

Urease is a nickel-dependent metalloenzyme that catalyzes the hydrolysis of urea to ammonia, thus neutralizing gastric acid and creating an alkaline local environment required for *Hp* survival.[34,35] The 3D coordinates of *Hp* urease were retrieved by Protein Data Bank (PDB ID 6ZJA).[36] Validation of the docking protocol was achieved by re-docking the cognate ligand DJM and obtaining a geometry with a docking score of −11.131 kcal mol^{-1} and an RMSD of 2.413 Å compared to the crystallographic ligand.

FabZ is a potent enzyme in fatty acid biosynthesis and catalyzes the dehydration of β-hydroxyacyl-ACP to *trans*-2-acyl-ACP.[37] The discovery of *Hp*-FabZ inhibitors is of special interest in the treatment of various gastric diseases.[38] The structure of the enzyme (PDB ID 3DOZ)[38] was prepared and minimized before performing docking simulations. A fundamental water molecule was maintained in the active site for interaction with the crystallographic ligand (docking score −5.491 kcal mol^{-1} and RMSD 0.8322 Å).

Hp G6PD is a key enzyme in the metabolism of *Hp*, particularly in the pentose phosphate pathway that provides NADH^{+}/ATP through glycolysis.[39] As the 3D coordinates of the bacterial G6PD are still unknown, the homology modeling tool in Maestro[40] was used to predict the structure of the enzyme. The primary sequence of the enzyme (strain ATCC 700392/26695) was used to identify the most suitable model in the Protein Data Bank[41] using BLAST.[42] *Leishmania donovani* G6PD (PDB ID 7ZHV)[43] with the best identity percentage (31.74%) was used as the template. The visual inspection of the docking poses of the azo derivatives in the active site of urease, FabZ, and G6PD and the obtained docking score values suggest that azo compounds do not interact with these targets.

IMPDH, a fundamental enzyme in the biosynthesis of purine nucleotides, is responsible for the oxidation of inosine 5′-monophosphate (IMP) to xanthosine 5′-monophosphate (XMP), which is further converted to guanosine 5′-monophosphate (GMP) by GMP synthase.[44] Inhibition of IMPDH reduces the guanine nucleotide pool, thereby inhibiting microbial proliferation. Given the fundamental differences between prokaryotic and eukaryotic IMPDH in terms of their structural and kinetic characteristics, it is possible to obtain selective inhibitors of the bacterial enzyme (selective toxicity). Consequently, *Hp*-IMPDH inhibitors can be developed as valid antimicrobial agents.[17] As the 3D structure of *Hp*-IMPDH is not yet known, it was modelled using the Homology Model tool of Maestro.[40] The primary sequence of *Hp*-IMPDH (strain ATCC 700392/26695) was used to identify the best template in the Protein Data Bank[41] using BLAST.[42] The optimal model, with 60.2% identity, was identified as *Campylobacter jejuni* (*Cj* strain ATCC 700819 IMPDH (*Cj*-IMPD)), and the available 3D structure of *Cj*-IMPD (PDB ID 4MZ1)[45] was employed as a template, including the IMP ligand. The modelled *Hp*-IMPDH was prepared and

Table 2 Antimicrobial activity (MIC and MBC values) of derivatives **20** and **28** against additional bacterial species

	MIC/MBC (μg mL^{-1})		
Cpd	*E. coli* ATCC 25922	*P. aeruginosa* ATCC 27853	*S. aureus* ATCC 29213
20	>128/>128	>128/>128	2/32
28	>128/>128	>128/>128	2/32

Open Access Article. Published on 09 October 2024. Downloaded on 10/27/2025 5:03:29 PM.
This article is licensed under a Creative Commons Attribution-NonCommercial 3.0 Unported Licence.

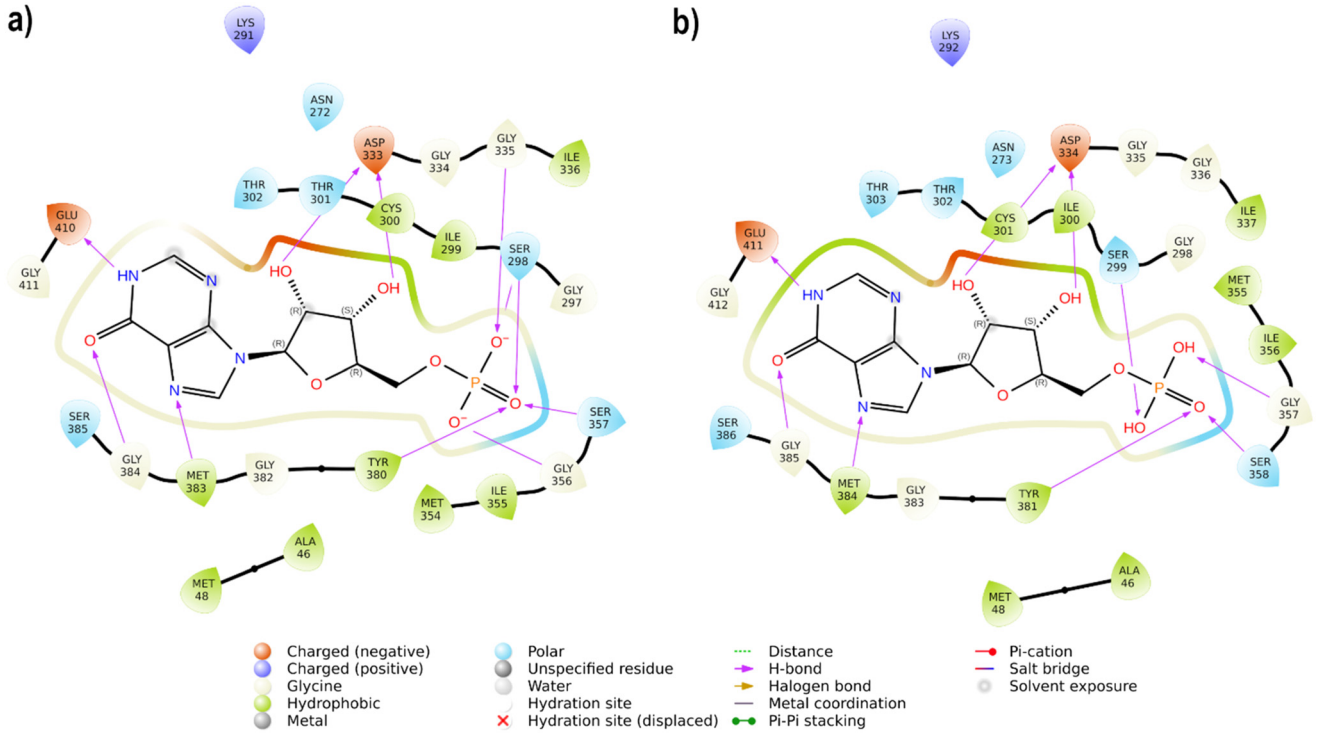

Fig. 2 (a) 2D interaction of IMP in the active site of modelled *Hp*-IMPDH, (b) 2D interaction of IMP in the active site of *Cj*-IMPDH (PDB ID 4MZ1).

minimized before docking analysis. In the active site of *Hp*-IMPDH, the IMP ligand forms hydrogen bond contacts with Ser298, Asp333, Gly335, Gly356, Ser357, Met383, Gly384, and Glu410, as illustrated in Fig. 2a. This pattern of interactions is consistent with that observed in *Cj*-IMPD (PDB ID 4MZ1), as shown in Fig. 2b.

The best-docked pose of IMP possesses a docking score of −9.045 kcal mol^{-1} and an RMSD of 0.8322 Å between the docked pose and the crystallographic ligand, confirming the validation of the protocol. The docking study of compounds **20** (docking score of −5.967 kcal mol^{-1}) and **28** (docking score of −6.370 kcal mol^{-1}) revealed that they are deeply inserted into the active site of IMPH, establishing a pattern of interactions similar to those of IMP. The nitro group of **20** interacts with Ser298 and Gly356 through H-bonds, while the hydroxyl group forms H-bonds with Asp244 (Fig. 3a and c). As the hydroxyl group of **28** is at the *ortho* position to the azo group, it is unable to reach Asp244, while the aromatic ring is involved in a cation–π interaction with Lys291. In addition, the nitro group is H-bonded to Ser298, Gly356, Ser357, and Tyr380 (Fig. 3b and d).

The nitrophenyl rings of **20** and **28** occupy the area typically occupied by the phosphate group of IMP, but the rigidity of the azo linker prevents the benzene ring from arranging like the purine ring of the IMP, projecting the phenol on the opposite side (Fig. 4). Nevertheless, favorable interactions are still present.

Given that the majority of IMPDH inhibitors act as non-competitive inhibitors,[46] a docking study was conducted to investigate the non-competitive binding of the most active compounds in *Hp*-IMPDH. The grid was constructed with IMP in the protein and the grid box was centered on the crystallographic ligand of *Cj*-IMPD. The docking results indicated that **28** can form a π–π interaction between the phenol ring and the purine moiety of IMP and a cation–π interaction between the nitrophenyl ring and Lys71, in accordance with the findings of other non-competitive inhibitors (Fig. 5). In conclusion, the docking study of the most active compounds in the active site of *Hp*-IMPDH revealed that they can act as competitive and non-competitive inhibitors. The obtained results suggest that *Hp*-IMPDH is a possible target of the studied compounds in the *Hp*, but further experimental studies are necessary to confirm our hypothesis.

2.4. *In silico* physicochemical and pharmacokinetic properties

The most promising compounds (**16**, **18**, **20**, **26**, and **28**) were selected for a *in silico* analysis of pharmacokinetic properties. For these purposes, the pkCSM web tool[47] was employed and the assessed chemical, ADME, drug-likeness, and toxicological properties are reported in Table 3.

All tested compounds exhibited high intestinal absorption (absorption >85%) as well as high permeability in human epithelial colorectal adenocarcinoma (Caco-2) cells, an index of intestinal permeability and efflux liability. Three of the selected compounds (**16**, **18**, and **26**) displayed values of logarithm of the apparent permeability coefficient ($\log P_{app}$) higher than 0.90, which is considered as the threshold value for high permeability, whereas derivatives **20** and **28** displayed $\log P_{app}$ of 0.36 and 0.40, respectively, accounting for moderate absorption.

Open Access Article. Published on 09 October 2024. Downloaded on 10/27/2025 5:03:29 PM.
This article is licensed under a Creative Commons Attribution-NonCommercial 3.0 Unported Licence.

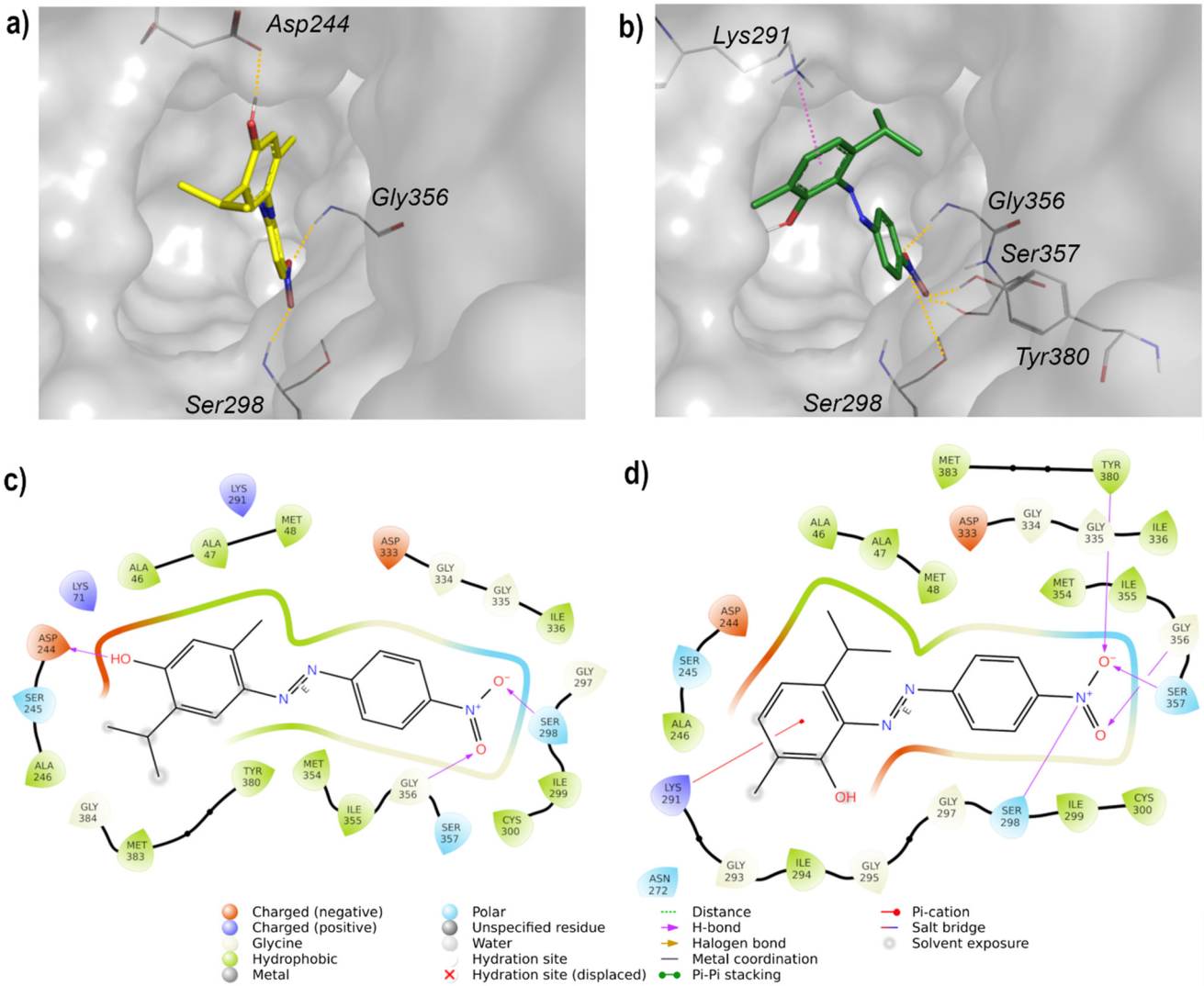

Fig. 3 3D interaction of **20** (a) and **28** (b) in the active site of modelled *Hp*-IMPDH; dotted orange line for H-bond, dotted violet line for cation–π. 2D interaction in the active site of modelled *Hp*-IMPDH of **20** (c) and **28** (d).

Although a good blood–brain barrier (BBB) permeability for the compounds was found to be in the negative range, with logarithmic ratio of brain to plasma drug concentration

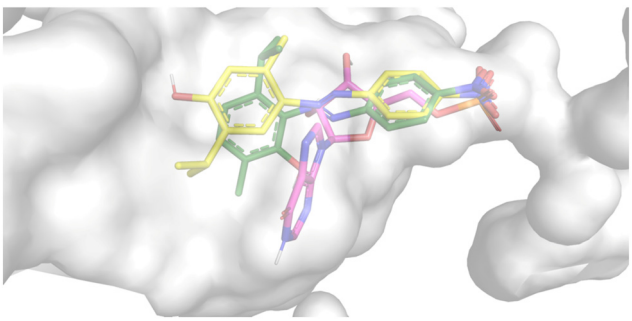

Fig. 4 Superimposition of IMP (magenta stick), **20** (yellow stick), and **28** (green stick) in the active site of modelled *Hp*-IMPDH represented as culled surface.

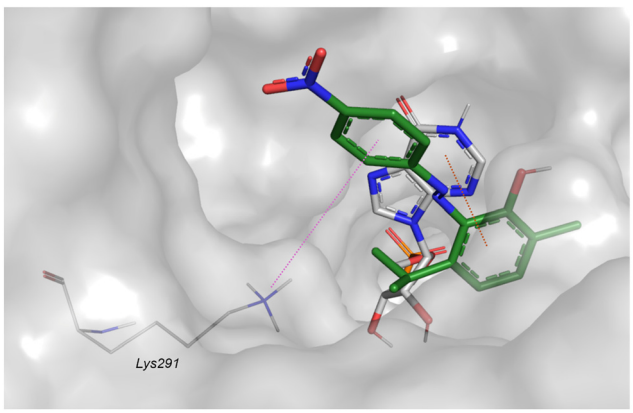

Fig. 5 Best docked pose of **28** (green stick) as a non-competitive ligand. IMP (grey stick), dotted violet line for cation–π, and dotted red line for π–π.

Open Access Article. Published on 09 October 2024. Downloaded on 10/27/2025 5:03:29 PM.
This article is licensed under a Creative Commons Attribution-NonCommercial 3.0 Unported Licence.

Table 3 ADME parameters were assessed through the pkCSM tool for compounds **16**, **18**, **20**, **26**, and **28**

Properties		Compounds				
		16	**18**	**20**	**26**	**28**
Absorption	Water solubility (log mol/L)	−5.918	−5.454	−4.978	−4.675	−4.937
	Caco-2 permeability expressed as log P_{app} in pkCSM 10^{-6} cm s^{-1}	1.485	1.396	0.364	1.363	0.4
	Intestinal absorption (human) (% adsorbed)	87.887	91.908	88.159	91.621	88.823
	Skin permeability (log K_P)	−2.231	−2.642	−2.732	−2.723	−2.737
	P-glycoprotein substrate	No	No	Yes	Yes	Yes
	P-glycoprotein I inhibitor	No	No	No	No	No
	P-glycoprotein II inhibitor	No	No	No	No	No
Distribution	Volume of distribution at steady state (VD_{ss}) (human) (log L/kg)	0.625	0.464	0.027	0.356	0.161
	Fraction unbound (human) (Fu)	0	0.003	0	0.022	0
	Blood–brain barrier (BBB) permeability (log BB)	0.002	−0.14	−0.167	−0.184	−0.264
	CNS permeability (log PS)	−1.452	−1.627	−1.638	−1.619	−1.664
Metabolism	CYP2D6 substrate	No	No	No	No	No
	CYP3A4 substrate	Yes	Yes	Yes	Yes	Yes
	CYP1A2 inhibitor	Yes	Yes	Yes	Yes	Yes
	CYP2C19 inhibitor	Yes	Yes	Yes	Yes	Yes
	CYP2C9 inhibitor	Yes	Yes	Yes	Yes	Yes
	CYP2D6 inhibitor	No	No	No	No	No
	CYP3A4 inhibitor	No	Yes	Yes	No	Yes
Excretion	Total clearance (log mL min^{-1} Kg)	0.104	−0.106	−0.095	−0.108	−0.111
	Renal organic cationic transporter (OCT2) substrate	No	No	No	No	No

(log BB) values <0.3, all analyzed derivatives were predicted to penetrate the central nervous system (CNS), resulting to be CNS-positive, with values of *in vivo* BBB permeability-surface area (log PS) ≥ −2. This discrepancy could be due to the different parameters considered to compute BBB permeability (measured *in vivo* as log BB) and CNS permeability (obtained from *in situ* brain perfusions with the compound directly injected into the carotid artery). On the other hand, considering the localization of the *Hp* in the stomach mucosa, the ability to penetrate the CNS is not a central issue for the anti-bacterial activity.

With regard to the metabolism, these compounds could act as a substrate or inhibit cytochrome P450 (CYP) 3A4. In particular, the tested compounds resulted in being a substrate for the CYP3A4 isoform, whereas compounds **18**, **20**, and **28** were predicted to inhibit this enzyme. In contra, compounds **16** and **26** did not show any inhibitory activity against CYP3A4. Interestingly, none of these compounds were found to be CYP2D6 isoform substrates or inhibitors. As stated above, the currently employed standard therapy for *Hp* eradication consists of triple therapy including PPIs, **CLR**, and **AMX**;[48] thereby, the development of drugs/drug candidates not interfering with the other drugs' metabolism could be useful to assess a potential co-administration in polytherapy.

2.5. Cell toxicity in normal cell lines

To evaluate the biological effects *in vitro* of **20** and **28**, increasing concentrations of these compounds were administered to human gastric epithelial SV40-immortalized non-tumorigenic, GES-1,[49] and normal epithelial cells from the small intestine, HIEC-6, up to 72 h of exposure (Fig. 6 and 7). These cell lines were chosen to overcome the limitations of the use of cancerous AGS, Caco-2, and HT-29 cell lines as *in vitro* models. In fact, GES-1 cells mimic the site of *H. pylori* infection and HIEC-6 polarized columnar cells represent a satisfactory alternative displaying human crypt-like features with dense microvilli and non-organized tight junctions.[50]

At 24 h, both compounds are well tolerated in the low–medium concentration range, with the IC_{50} assessed at 14.99

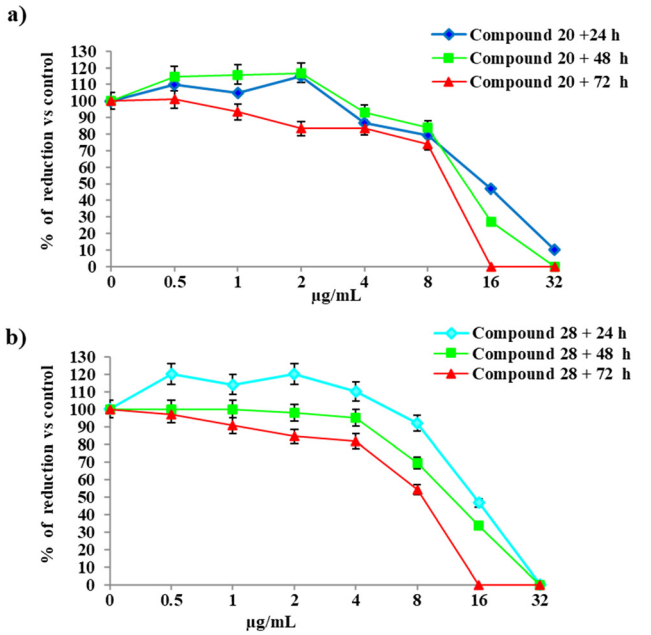

Fig. 6 Cell viability after treatment with compounds **20** and **28** by Alamar blue assay. GES-1 cells were incubated for 24, 48, and 72 h with different concentrations of **20** (a) and **28** (b). The untreated control (untreated cells) was set as 100%. The percent reduction of Alamar blue in the treated and untreated samples was calculated with the formula indicated by the manufacturer.

Open Access Article. Published on 09 October 2024. Downloaded on 10/27/2025 5:03:29 PM.
This article is licensed under a Creative Commons Attribution-NonCommercial 3.0 Unported Licence.

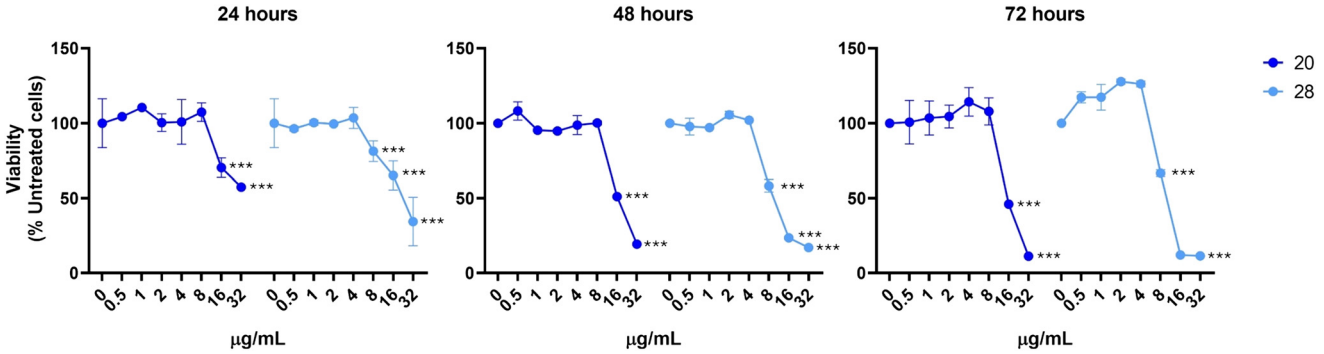

Fig. 7 Cell viability of HIEC-6 cells in the presence of **20** and **28** after 24, 48, and 72 h of exposure. Trend lines represent percentages of cell viability. The untreated control (untreated cells) was set as 100%. ***$p < 0.0001$ between cells exposed to compounds and the untreated control.

μg mL^{-1} and 12.09 μg mL^{-1} for **20** and **28**, respectively, in GES-1, and at 15.06 μg mL^{-1} and 13.60 μg mL^{-1}, respectively, on HIEC-6 cells. Notably, the IC_{50} values obtained were significantly higher than the concentrations obtained as MICs for both compounds. At 48 h and 72 h, compound **28** was characterized by a major toxicity on HIEC-6 cells, with the IC_{50} assessed at 7.61 μg mL^{-1}. On GES-1 cells the toxicity increased only at 72 h with the IC_{50} of 8.44 μg mL^{-1}. In parallel, the cell viability trend in the presence of **20** is comparable with the one registered at 24 h on both cell lines. In particular, on GES-1 the IC_{50} at 48 h and 72 h was 12.09 μg mL^{-1} and 12.02 μg mL^{-1}, respectively; at 48 h and 72 h, HIEC-6 showed an IC_{50} of 13.38 μg mL^{-1} and 13.26 μg mL^{-1}, respectively. In conclusion, the discrete selective toxicity of these compounds, calculated as the IC_{50}/MIC_{50} ratio, corroborates their further refinement for the design of new and selective anti-*H. pylori* agents.

3. Conclusions

In the frame of increasing antimicrobial resistance phenomena and the correlated decrease in efficacy of the current drugs, the search for new compounds with innovative mechanisms of action is recommended. For a long time, we have put great effort into the development of potent and broad-spectrum antibiotics,[51–54] especially towards *Hp*,[55] a pathogen threatening public health due to the associated severe diseases. Herein, we reported a series of 36 compounds resulting from the classical diazotization reaction of such phenols with structurally diverse aromatic amines. Interestingly, for **Car** and **Thy**, apart from the expected *para*-azo derivatives, being the sterically preferred isomers, disubstituted compounds with an *ortho*- and *para*-substitution pattern were also obtained, and in just one case, we succeeded to isolate the **Car** *ortho*-azo derivative (**20**). Notably, the *O*-modified compounds **29–36** showed a complete loss of activity with respect to the corresponding free phenols **26** and **28**, being among the most active and selective compounds in the series, thereby confirming the importance of the free phenolic group for the antibacterial activity. However, the mono-azo compounds resulted in exerting an anti-*Hp* activity, with Eu derivatives exerting the weakest activity or being totally inactive, whereas compounds generated from **Van**, **Car**, and **Thy** showed different bioactivity based on the aromatic amine-derived substituents. Likely due to the highest steric hindrance, the bis-azo derivatives resulted in not inhibiting the *Hp* growth.

To search a putative target for this class of compounds, we investigated *Hp* urease, FabZ, G6PD, and IMPDH, being the most extensively studied *Hp* targets through reverse docking calculations by using homology models when required. Promising results were obtained with compounds **20** and **28** in the IMPDH active site acting as competitive or non-competitive ligand. Interestingly, the IMPDH enzyme is involved in microbial proliferation; thereby its inhibition could interfere with bacterial growth. In the end, a new series of 36 compounds derived from diazotization of phenolic monoterpenes has been designed and synthesized as selective and quite safe antibacterial agents active against *Hp*, and a pharmacological target has been suggested by *in silico* studies. Further investigations are necessary to confirm it and address the synthesis toward more potent antibacterial agents.

4. Materials and methods

4.1. Chemistry

General chemistry. All commercially available monoterpenes and their analogues, chemicals, and solvents were purchased from Merck (Milan, Italy) and used as purchased. Chromatographic separations were performed on columns packed with silica gel (230–400 mesh, for flash technique). Reaction monitoring was performed through thin-layer chromatography (TLC) by using 0.2 mm-thick silica gel–aluminium-backed plates (60, F254). TLC spot visualization was performed under short and long wavelength (254 and 365 nm, respectively) ultraviolet irradiation and stained with ninhydrin or basic permanganate by dipping and heating with a hot air gun. ^{1}H and ^{13}C NMR spectra were recorded on a spectrometer operating at 300/400/600 and 75/100/151 MHz, respectively. Spectra were reported in parts per million (δ scale) and internally referenced to the $CDCl_3$, CD_3-OD, or DMSO-d_6 signal at δ 7.26, 3.31, and 2.50 ppm,

Open Access Article. Published on 09 October 2024. Downloaded on 10/27/2025 5:03:29 PM.
This article is licensed under a Creative Commons Attribution-NonCommercial 3.0 Unported Licence.

respectively. Chemical shifts for carbon are reported in parts per million (δ scale) and referenced to the carbon resonances of the solvent ($CDCl_3$ at δ 77.0, CD_3OD at δ 49.0, DMSO-d_6 at δ 39.0). Data are shown as follows: chemical shift, multiplicity (s = singlet, d = doublet, t = triplet, q = quartet, qi = quintet, m = multiplet and/or multiplet resonances, br = broad signal, ap = apparent), integration and coupling constants (J) in hertz (Hz). The ^{1}H and ^{13}C spectra confirmed the anticipated number of hydrogens and carbons for each compound, respectively. Melting points were measured on a Stuart® melting point apparatus SMP1 (Fisher Scientific Italia, Segrate (MI), Italy) and are uncorrected (temperatures are reported in °C). Elemental analyses for C, H, and N were recorded on a Perkin-Elmer 240 B microanalyzer (Perkin-Elmer, Waltham, MA, USA) and the analytical results are within ±0.4% of the theoretical values for all compounds.

Synthetic procedure and characterization data. An acid solution (conc. HCl/H_2O 1/10 mL) of the appropriate substituted aromatic amine (6.6 mmol) was added to a stirred aqueous solution of sodium nitrite (9.9 mmol in 5 mL of H_2O) at 0–5 °C (ice bath). The formed diazonium salt was allowed to couple by adding a mixture of the suitable phenol (6.6 mmol) in an aqueous solution of NaOH (6.6 mmol in 5 mL of H_2O), maintaining the pH value in the range from 8 to 9. When the reaction was complete, the mixture was poured into water (50 mL) and extracted with DCM three times. The combined organic layers were dried over anhydrous Na_2SO_4, filtered, and evaporated *in vacuo*. Silica gel column chromatography allowed the obtainment of the desired compound (eluent: *n*-hexane/ethyl acetate). The compounds were further purified by recrystallization from a 20–50% EtOH–water mixture.

(E)-4-Allyl-2-methoxy-6-(o-tolyldiazenyl)phenol ***(1)***. Brown solid, m.p. 82–85 °C, 69% yield. ^{1}H NMR (600 MHz, $CDCl_3$) δ 2.62 (s, 3H, Ar–CH_3) 3.43 (d, J = 6.0 Hz, 2H, Ar–CH_2), 3.94 (s, 3H, OCH_3), 5.11–5.17 (m, 2H, ═CH_2), 5.98–6.05 (m, 1H, ═CH), 6.81 (d, J = 6.0 Hz, 1H, Ar), 7.33–7.35 (m, 1H, Ar), 7.35–7.38 (m, 2H, Ar), 7.43 (d, J = 3.0 Hz, 1H, Ar), 7.83 (d, J = 6.0 Hz, 1H, Ar). ^{13}C NMR (151 MHz, $CDCl_3$) δ 18.1, 39.7, 56.5, 115.3, 115.7, 116.3, 124.1, 127.0, 130.7, 131.3, 131.5, 136.4, 137.3, 137.4, 142.0, 148.5, 148.9. Anal. calcd for $C_{17}H_{18}N_2O_2$: C, 72.32; H, 6.43; N, 9.92. Found: C, 72.29; H, 6.41; N, 9.95.

(E)-4-Allyl-2-methoxy-6-((3-methoxyphenyl)diazenyl)phenol ***(2)***. Brown solid, m.p. 105–107 °C, 71% yield. ^{1}H NMR (600 MHz, $CDCl_3$) δ 3.42 (d, J = 6.0 Hz, 2H, Ar–CH_2), 3.89 (s, 3H, OCH_3), 3.93 (s, 3H, OCH_3), 5.11–5.16 (m, 2H, ═CH_2), 5.99–6.03 (m, 1H, ═CH), 6.81 (d, J = 6.0 Hz, 1H, Ar), 7.04 (dq, 1H, Ar), 7.39–7.41 (m, 1H, Ar), 7.41–7.43 (m, 1H, Ar), 7.44 (d, J = 6.0 Hz, 1H, Ar), 7.45–7.47 (m, 1H, Ar). ^{13}C NMR (151 MHz, $CDCl_3$) δ 39.7, 55.6, 56.6, 104.9, 115.7, 116.3, 116.8, 118.0, 124.0, 130.2, 130.8, 137.0, 137.2, 141.9, 148.8, 151.7, 160.7. Anal. calcd for $C_{17}H_{18}N_2O_3$: C, 68.44; H, 6.08; N, 9.39. Found: C, 68.47; H, 6.09; N, 9.41.

(E)-4-Allyl-2-methoxy-6-((3-nitrophenyl)diazenyl)phenol ***(3)***. Red solid, m.p. 112–113 °C, 68% yield.^{1}H NMR (600 MHz, $CDCl_3$) δ 3.43 (dtd, J = 6.7, 1.5, 0.7 Hz, 2H, Ar–CH_2), 3.94 (s, 3H, OCH_3), 5.09–5.22 (m, 2H, ═CH_2), 5.96–6.06 (m, 1H, CH═), 6.86 (d, J = 2.0 Hz, 1H, Ar), 7.44 (dd, J = 1.9, 0.9 Hz, 1H, Ar), 7.71 (t, J = 8.0 Hz, 1H, Ar), 8.18 (ddd, J = 7.9, 1.9, 1.0 Hz, 1H, Ar), 8.32 (ddd, J = 8.2, 2.3, 1.0 Hz, 1H, Ar), 8.69 (t, J = 2.1 Hz, 1H, Ar). ^{13}C NMR (151 MHz, $CDCl_3$) δ 39.6, 56.6, 116.0, 116.6, 116.8, 124.2, 125.0, 129.0, 130.4, 131.4, 136.9, 137.2, 141.9, 148.9, 149.3, 151.3. Anal. calcd for $C_{16}H_{15}N_3O_4$: C, 61.34; H, 4.83; N, 13.41. Found: C, 61.38; H, 4.85; N, 13.44.

(E)-4-Allyl-2-methoxy-6-((4-nitrophenyl)diazenyl)phenol ***(4)***. Red-brown solid, m.p. 193–194 °C, 53% yield. ^{1}H NMR (600 MHz, $CDCl_3$) δ 3.43 (ddq J = 6.7, 1.5, 0.7 Hz, 2H, Ar–CH_2), 3.94 (s, 3H, OCH_3), 5.12–5.16 (m, 2H, ═CH_2), 5.96–6.06 (m, 1H, ═CH), 6.86 (d, J = 2.0 Hz, 1H, Ar), 7.43–7.47 (m, 1H, Ar), 7.70 (d, J = 8.0 Hz, 1H, Ar), 8.18 (ddd, J = 7.9, 2.0, 1.0 Hz, 1H, Ar), 8.32 (ddd, J = 8.2, 2.3, 1.0 Hz, 1H, Ar), 8.69 (t, J = 2.1 Hz, 1H, Ar). ^{13}C NMR (151 MHz, $CDCl_3$) δ 39.6, 56.6, 116.0, 116.6, 124.2, 125.0, 128.9, 130.4, 131.4, 136.9, 137.2, 142.0, 148.9, 149.3, 151.3. Anal. calcd for $C_{16}H_{15}N_3O_4$: C, 61.34; H, 4.83; N, 13.41. Found: C, 61.30; H, 4.82; N, 13.43.

(E)-4-Allyl-2-((2,4-dichlorophenyl)diazenyl)-6-methoxyphenol ***(5)***. Red solid, m.p. 137–139 °C, 54% yield. ^{1}H NMR (300 MHz, $CDCl_3$) δ 3.42 (d, J = 6.6 Hz, 2H, Ar–CH_2), 3.94 (s, 3H, OCH_3), 5.12–5.18 (m, 2H, ═CH_2), 5.95–6.08 (m, 1H, CH═), 6.84 (d, J = 1.2 Hz, 1H, Ar), 7.33–7.40 (m, 2H, Ar), 7.58 (d, J = 1.8 Hz, 1H, Ar), 7.87 (d, J = 9.0 Hz, 1H, Ar), 13.18 (s, 1H, OH). ^{13}C NMR (151 MHz, $CDCl_3$) δ 39.5, 56.5, 116.2, 116.3, 118.0, 124.3, 128.1, 130.3, 130.9, 134.6, 136.9, 137.3, 137.6, 141.9, 149.0. Anal. calcd for $C_{16}H_{14}Cl_2N_2O_2$: C, 56.99; H, 4.18; N, 8.31. Found: C, 56.94; H, 4.15; N, 8.28.

(E)-4-Allyl-2-(benzo[d][1,3]dioxol-5-yldiazenyl)-6-methoxyphenol ***(6)***. Brown solid, m.p. 142–144 °C, 73% yield. ^{1}H NMR (600 MHz, $CDCl_3$) δ 3.42 (d, J = 6.0 Hz, 2H, Ar–CH_2), 3.93 (s, 3H, OCH_3), 5.10–5.17 (m, 2H, ═CH_2), 5.97–6.06 (m, 1H, CH═), 6.07 (s, 2H, OCH_2O), 6.79 (s, 1H, Ar), 6.93 (d, J = 9.0 Hz, 1H, Ar), 7.35 (s, 1H, Ar), 7.42 (s, 1H, Ar), 7.43 (s, 1H, Ar). ^{13}C NMR (151 MHz, $CDCl_3$) δ 39.7, 56.5, 98.6, 102.2, 108.3, 115.1, 116.2, 122.6, 123.6, 130.7, 136.9, 137.3, 141.2, 146.4, 148.7, 149.2, 150.6. Anal. calcd for $C_{17}H_{16}N_2O_4$: C, 65.38; H, 5.15; N, 8.97. Found: C, 65.35; H, 5.17; N, 9.00.

(E)-4-Allyl-2-methoxy-6-(naphthalen-1-yldiazenyl)phenol ***(7)***. Brown solid, m.p. 113–115 °C, 68% yield. ^{1}H NMR (600 MHz, $CDCl_3$) δ 3.45 (dtd, J = 6.7, 1.4, 0.7 Hz, 2H, Ar–CH_2), 3.97 (s, 3H, OCH_3), 5.10–5.21 (m, 2H, ═CH_2), 6.03 (ddt, J = 16.8, 10.0, 6.7 Hz, 1H, CH═), 6.84 (d, J = 2.0 Hz, 1H, Ar), 7.49 (dd, J = 1.8, 0.9 Hz, 1H, Ar), 7.54–7.64 (m, 2H, Ar), 7.63 (ddd, J = 8.4, 6.8, 1.4 Hz, 1H, Ar), 7.94 (ddt, J = 8.1, 1.3, 0.6 Hz, 1H, Ar), 7.98 (ddd, J = 10.6, 7.9, 1.1 Hz, 2H, Ar), 8.50 (dq, J = 8.6, 0.9 Hz, 1H, Ar). ^{13}C NMR (151 MHz, $CDCl_3$) δ 39.8, 56.6, 113.3, 115.6, 116.4, 122.2, 124.0, 125.9, 126.8, 127.7, 128.5, 129.6, 131.0, 131.7, 134.4, 137.2, 137.9, 142.1, 145.9, 148.9. Anal. calcd for $C_{20}H_{18}N_2O_2$: C, 75.45; H, 5.70; N, 8.90. Found: C, 75.49; H, 5.73; N, 8.93.

(E)-3-((2-Chlorophenyl)diazenyl)-4-hydroxy-5-methoxybenzaldehyde ***(8)***. Brown solid, m.p. 200–202 °C, 56% yield. Characterization data are in agreement with previous literature.[56] Anal. calcd for $C_{14}H_{11}ClN_2O_3$: C, 57.84; H, 3.81; N, 9.64. Found: C, 57.88; H, 3.83; N, 9.66.

Open Access Article. Published on 09 October 2024. Downloaded on 10/27/2025 5:03:29 PM. This article is licensed under a Creative Commons Attribution-NonCommercial 3.0 Unported Licence.

*(E)-3-((3-Chlorophenyl)diazenyl)-4-hydroxy-5-methoxybenzaldehyde (**9**).* Red-brown solid, m.p. 180–182 °C, 72% yield. Characterization data are in agreement with previous literature.[56] Anal. calcd for $C_{14}H_{11}ClN_2O_3$: C, 57.84; H, 3.81; N, 9.64. Found: C, 57.81; H, 3.79; N, 9.67.

*(E)-4-Hydroxy-3-methoxy-5-((3-nitrophenyl)diazenyl)benzaldehyde (**10**).* Red-brown solid, m.p. 112–113 °C, 76% yield. Characterization data are in agreement with previous literature.[57] Anal. calcd for $C_{14}H_{11}N_3O_5$: C, 55.82; H, 3.68; N, 13.95. Found: C, 55.85; H, 3.70; N, 13.98.

*(E)-4-Hydroxy-3-methoxy-5-(p-tolyldiazenyl)benzaldehyde (**11**).* Red solid, m.p. 82–84 °C, 90% yield. Characterization data are in agreement with previous literature.[57] Anal. calcd for $C_{15}H_{14}N_2O_3$: C, 66.66; H, 5.22; N, 10.36. Found: C, 66.70; H, 5.24; N, 10.39.

*(E)-4-Hydroxy-3-methoxy-5-((4-methoxyphenyl)diazenyl) benzaldehyde (**12**).* Orange solid, m.p. 82–83 °C, 66% yield. Characterization data are in agreement with previous literature.[58] Anal. calcd for $C_{15}H_{14}N_2O_4$: C, 62.93; H, 4.93; N, 9.79. Found: C, 62.96; H, 4.95; N, 9.77.

*(E)-3-((4-Bromophenyl)diazenyl)-4-hydroxy-5-methoxybenzaldehyde (**13**).* Red solid, m.p. 176–178 °C, 76% yield. ^{1}H NMR (600 MHz, $CDCl_3$) δ 4.03 (s, 3H, OCH_3), 7.53 (d, J = 2.4 Hz, 1H, Ar), 7.72 (dt, J = 13.5, 3.3 Hz, 2H, Ar), 7.79 (dt, J = 9.9, 3.6 Hz, 2H, Ar), 8.10 (d, J = 3.0 Hz, 1H, Ar), 9.97 (s, 1H, CHO). ^{13}C NMR (151 MHz, $CDCl_3$) δ 56.6, 111.0, 123.8, 126.5, 128.7, 130.3, 132.9, 149.7. Anal. calcd for $C_{14}H_{11}BrN_2O_3$: C, 50.17; H, 3.31; N, 8.36. Found: C, 50.20; H, 3.33; N, 8.39.

*(E)-4-((5-Formyl-2-hydroxy-3-methoxyphenyl)diazenyl)benzonitrile (**14**).* Brown solid, m.p. 203–204 °C, 90% yield. ^{1}H NMR (300 MHz, $CDCl_3$) δ 4.01 (s, 3H, OCH_3), 7.53 (s, 1H, Ar), 7.86 (d, J = 8.7 Hz, 2H, Ar), 7.99 (d, J = 8.1 Hz, 2H, Ar), 8.01 (d, J = 1.8 Hz, 1H, Ar), 9.96 (s, 1H, CHO), 13.69 (s, 1H, OH). ^{13}C NMR (75 MHz, $CDCl_3$) δ 56.6, 111.7, 114.8, 118.0, 122.8, 129.0, 130.5, 133.6, 136.4, 150.2, 151.7, 189.8. Anal. calcd for $C_{15}H_{11}N_3O_3$: C, 64.05; H, 3.94; N, 14.94. Found: C, 64.09; H, 3.96; N, 14.91.

*(E)-3-((3,4-Dichlorophenyl)diazenyl)-4-hydroxy-5-methoxybenzaldehyde (**15**).* Red-brown solid, m.p. 188–190 °C, 81% yield. ^{1}H NMR (300 MHz, $CDCl_3$) δ 4.01 (s, 3H, OCH_3), 7.52 (s, 1H, Ar), 7.63 (d, J = 8.7 Hz, 1H, Ar), 7.76 (dd, J = 8.7, 2.0 Hz, 1H, Ar), 8.08 (dd, J = 22.8, 1.8 Hz, 2H, Ar), 9.95 (s, 1H, CHO), 13.48 (s, 1H, OH). ^{13}C NMR (75 MHz, $CDCl_3$) δ 56.6, 111.4, 122.3, 123.2, 128.8, 130.2, 131.3, 134.2, 136.0, 136.1, 148.8, 149.3, 150.0, 189.9. Anal. calcd for $C_{14}H_{10}Cl_2N_3O_3$: C, 51.72; H, 3.10; N, 8.62. Found: C, 51.75; H, 3.12; N, 8.65.

*(E)-4-((2-Chlorophenyl)diazenyl)-5-isopropyl-2-methylphenol (**16**).* Orange solid, m.p. 162–163 °C, 70% yield. ^{1}H NMR (400 MHz, DMSO) δ 1.27 (d, J = 6.8 Hz, 6H, 2 iPr CH_3), 2.15 (s, 3H, Ar–CH_3), 4.02–4.08 (m, 1H, iPr CH), 6.90 (s, 1H, Ar), 7.44–7.49 (m, 2H, Ar), 7.51 (s, 1H, Ar), 7.58–7.60 (m, 1H, Ar), 7.65–7.67 (m, 1H, Ar), 10.28 (s, 1H, OH). ^{13}C NMR (100 MHz, $CDCl_3$) δ 17.2, 22.4, 27.2, 115.2, 117.2, 117.9, 127.2, 130.5, 130.6, 133.0, 134.6, 138.7, 145.5, 149.3, 156.3. Anal. calcd for $C_{16}H_{17}ClN_2O$: C, 66.55; H, 5.93; N, 9.70. Found: C, 66.59; H, 5.91; N, 9.67.

*2,4-Bis((E)-(2-chlorophenyl)diazenyl)-3-isopropyl-6-methylphenol (**17**).* Brown solid, m.p. 109–111 °C, 15% yield. ^{1}H NMR (500 MHz, $CDCl_3$) δ 1.66 (d, J = 8.5 Hz, 6H, 2 iPr CH_3), 2.37 (d, J = 0.5 Hz, 3H, Ar–CH_3), 4.88–4.94 (m, 1H, iPr CH), 7.38–7.41 (m, 2H, Ar), 7.45–7.49 (m, 2H, Ar), 7.59–7.65 (m, 2H, Ar), 7.71–7.74 (m, 1H, Ar), 7.95 (s, 1H, Ar), 7.98–8.01 (m, 1H, Ar), 15.31 (s, 1H, OH). ^{13}C NMR (125 MHz, $CDCl_3$) δ 15.6, 24.4, 26.9, 117.7, 118.0, 127.3, 127.9, 130.8, 130.8, 131.0, 131.6, 133.4, 135.1, 146.0, 149.0, 150.0. Anal. calcd for $C_{22}H_{20}Cl_2N_4O$: C, 61.83; H, 4.72; N, 13.11. Found: C, 61.86; H, 4.75; N, 13.13.

*(E)-5-Isopropyl-4-((4-methoxyphenyl)diazenyl)-2-methylphenol (**18**).* Orange solid, m.p. 110–112 °C, 60% yield. ^{1}H NMR (400 MHz, DMSO) δ 1.26 (d, J = 6.8 Hz, 6H, 2 iPr CH_3), 2.14 (s, 3H, Ar–CH_3), 3.85 (s, 3H, OCH_3), 3.98–4.03 (m, 1H, iPr CH), 6.86 (s, 1H, Ar), 7.10 (d, J = 9.2 Hz, 2H, Ar), 7.46 (s, 1H, Ar), 7.80 (d, J = 8.8 Hz, 2H, Ar). ^{13}C NMR (100 MHz, DMSO) δ 16.1, 24.3, 27.3, 56.0, 112.0, 115.0, 117.6, 122.9, 124.3, 142.0, 147.4, 147.9, 159.4, 161.4. Anal. calcd for $C_{17}H_{20}N_2O_2$: C, 71.81; H, 7.09; N, 9.85. Found: C, 71.78; H, 7.06; N, 9.81.

*3-Isopropyl-2,4-bis((E)-(4-methoxyphenyl)diazenyl)-6-methylphenol (**19**).* Orange solid, m.p. 206–208 °C, 19% yield. ^{1}H NMR (600 MHz, $CDCl_3$) δ 1.66 (d, J = 10.8 Hz, 6H, 2× iPr CH_3), 2.34 (d, J = 1.2 Hz, 3H, Ar–CH_3), 3.89 (s, 3H, OCH_3), 3.90 (s, 3H, OCH_3), 4.83–4.94 (m, 1H, iPr CH), 7.03–7.07 (m, 4H, Ar), 7.77 (s, 1H, Ar), 7.86–7.90 (m, 2H, Ar), 7.93–7.96 (m, 2H, Ar). ^{13}C NMR (151 MHz, $CDCl_3$) δ 15.4, 24.2, 26.8, 55.6, 55.6, 114.2, 114.7, 122.3, 124.0, 124.6, 125.6, 134.2, 143.2, can144.4, 147.5, 147.6, 155.3, 161.4, 162.0. Anal. calcd for $C_{24}H_{26}N_4O_3$: C, 68.88; H, 6.26; N, 13.39. Found: C, 68.90; H, 6.28; N, 13.42.

*(E)-3-Isopropyl-6-methyl-2-((4-nitrophenyl)diazenyl)phenol (**20**).* Orange solid, m.p. 103–105 °C, 64% yield. ^{1}H NMR (300 MHz, $CDCl_3$) δ 1.36 (d, J = 6.6 Hz, 6H, 2 iPr CH_3), 2.22 (s, 3H, Ar–CH_3), 3.96–4.06 (m, 1H, iPr CH), 6.88 (d, J = 7.2 Hz, 1H, Ar), 7.27 (d, J = 7.2 Hz, 1H, Ar), 7.94 (d, J = 8.1 Hz, 2H, Ar), 8.39 (d, J = 8.1 Hz, Ar). ^{13}C NMR (151 MHz, $CDCl_3$) δ 15.0, 24.0, 28.0, 116.5, 122.4, 125.1, 137.2, 150.4, 154.2. Anal. calcd for $C_{16}H_{17}N_3O_3$: C, 64.20; H, 5.72; N, 14.04. Found: C, 64.24; H, 5.73; N, 14.05.

*2,4-Bis((E)-(4-bromophenyl)diazenyl)-3-isopropyl-6-methylphenol (**21**).* Brown solid, m.p. 218–220 °C, 18% yield. ^{1}H NMR (500 MHz, $CDCl_3$) δ 1.62 (d, J = 9.0 Hz, 6H, 2 iPr CH_3), 2.33 (s, 3H, Ar–CH_3), 4.82–4.86 (m, 1H, iPr CH), 7.67–7.73 (m, 4H, Ar), 7.78–7.85 (m, 5H, Ar), 14.99 (s, 1H, OH). ^{13}C NMR (125 MHz, $CDCl_3$) δ 15.3, 24.3, 26.8, 123.5, 124.3, 124.6, 125.3, 126.3, 132.9, 148.8, 149.4, 151.6. Anal. calcd for $C_{22}H_{20}Br_2N_4O$: C, 51.19; H, 3.91; N, 10.85. Found: C, 51.15; H, 3.90; N, 10.87.

*(E)-2-Isopropyl-5-methyl-4-(o-tolyldiazenyl)phenol (**22**).* Orange solid, m.p. 110–111 °C, 60% yield. Characterization data are in agreement with previous literature.[59] Anal. calcd for $C_{17}H_{20}N_2O$: C, 76.09; H, 7.51; N, 10.44. Found: C, 76.13; H, 7.53; N, 10.42.

*6-Isopropyl-3-methyl-2,4-bis((E)-o-tolyldiazenyl)phenol (**23**).* Brown solid, m.p. 143–145 °C, 20% yield. ^{1}H NMR (500 MHz,

Open Access Article. Published on 09 October 2024. Downloaded on 10/27/2025 5:03:29 PM. This article is licensed under a Creative Commons Attribution-NonCommercial 3.0 Unported Licence.

$CDCl_3$) δ 1.23 (d, J = 8.5 Hz, 6H, 2 iPr CH_3), 2.59 (s, 3H, Ar–CH_3), 2.67 (s, 3H, Ar–CH_3), 3.06 (s, 3H, Ar–CH_3), 3.33–3.36 (m, 1H, iPr CH), 7.17–7.29 (m, 6H, Ar), 7.59 (d, J = 9.5 Hz, 1H, Ar), 7.81–7.84 (m, 2H, Ar), 15.30 (s, 1H, OH). ^{13}C NMR (125 MHz, $CDCl_3$) δ 11.6, 17.7, 18.3, 22.4, 26.5, 115.9, 116.3, 119.2, 126.4, 127.1, 130.1, 130.7, 131.2, 131.5, 135.4, 136.2, 137.5, 140.8, 143.8, 151.1, 156.5. Anal. calcd for $C_{24}H_{26}N_4O$: C, 74.58; H, 6.78; N, 14.50. Found: C, 74.61; H, 6.80; N, 14.52.

*(E)-4-((2-Chlorophenyl)diazenyl)-2-isopropyl-5-methylphenol (**24**).* Orange solid, m.p. 182–183 °C, 70% yield. ^{1}H NMR (600 MHz, $CDCl_3$) δ 1.32 (d, J = 10.8 Hz, 6H, 2 iPr CH_3), 2.69 (s, 3H, Ar–CH_3), 3.17–3.24 (m, 1H, iPr CH), 5.25 (s, 1H, OH), 7.33–7.36 (m, 2H, Ar), 7.55–7.57 (m, 1H, Ar), 7.65–7.66 (m, 1H, Ar), 7.77 (s, 1H, Ar). ^{13}C NMR (151 MHz, $CDCl_3$) δ 17.2, 22.4, 27.2, 115.2, 117.2, 117.9, 127.2, 130.5, 130.6, 133.0, 134.6, 138.7, 145.5, 149.3, 156.3. Anal. calcd for $C_{16}H_{17}ClN_2O$: C, 66.55; H, 5.93; N, 9.70. Found: C, 66.51; H, 5.91; N, 9.73.

*2,4-Bis((E)-(2-chlorophenyl)diazenyl)-6-isopropyl-3-methylphenol (**25**).* Brown solid, m.p. 188–190 °C, 16% yield. ^{1}H NMR (500 MHz, $CDCl_3$) δ 1.35 (d, J = 8.5 Hz, 6H, 2 iPr CH_3), 3.14 (s, 3H, Ar–CH_3), 3.45–3.47 (m, 1H, iPr CH), 7.36–7.38 (m, 2H, Ar), 7.41–7.44 (m, 2H, Ar), 7.56–7.59 (m, 2H, Ar), 7.73–7.75 (m, 1H, Ar), 8.00–8.03 (m, 2H, Ar), 15.19 (s, 1H, OH). ^{13}C NMR (125 MHz, $CDCl_3$) δ 11.6, 22.2, 26.5, 117.7, 117.9, 120.4, 127.2, 127.7, 130.5, 130.6, 130.9, 131.4, 133.0, 134.9, 135.4, 136.8, 141.8, 143.7, 145.8, 149.0, 157.2. Anal. calcd for $C_{22}H_{20}Cl_2N_4O$: C, 61.83; H, 4.72; N, 13.11. Found: C, 61.80; H, 4.70; N, 13.14.

*(E)-2-Isopropyl-4-((4-methoxyphenyl)diazenyl)-5-methylphenol (**26**).* Yellow solid, m.p. 88–90 °C, 58% yield. Characterization data are in agreement with previous literature.[57] Anal. calcd for $C_{17}H_{20}N_2O_2$: C, 71.81; H, 7.09; N, 9.85. Found: C, 71.78; H, 7.07; N, 9.82.

*6-Isopropyl-2,4-bis((E)-(4-methoxyphenyl)diazenyl)-3-methylphenol (**27**).* Brown solid, m.p. 186–187 °C, 30% yield. ^{1}H NMR (600 MHz, $CDCl_3$) δ 1.35 (d, J = 10.8 Hz, 6H, 2 iPr CH_3), 3.10 (s, 3H, Ar–CH_3), 3.41–3.45 (m, 1H, iPr CH), 3.92 (s, 3H, OCH_3), 3.92 (s, 3H, OCH_3), 7.03–7.06 (m, 4H, Ar), 7.85 (s, 1H, Ar), 7.91 (dd, J = 10.2, 1.8 Hz, 2H, Ar), 7.97 (dd, J = 10.2, 1.5 Hz, 2H, Ar), 14.92 (s, 1H, OH). ^{13}C NMR (151 MHz, $CDCl_3$) δ 11.6, 22.4, 26.7, 55.6, 55.7, 114.1, 114.7, 117.8, 123.9, 124.5, 134.7, 135.5, 139.7, 143.4, 144.5, 147.5, 154.3, 161.4, 162.0. Anal. calcd for $C_{24}H_{26}N_4O_3$: C, 68.88; H, 6.26; N, 13.39. Found: C, 68.91; H, 6.28; N, 13.41.

*(E)-2-Isopropyl-5-methyl-4-((4-nitrophenyl)diazenyl)phenol (**28**).* Orange solid, m.p.: 176–177 °C, 74% yield. Characterization data are in agreement with previous literature.[59] Anal. calcd for $C_{16}H_{17}N_3O_3$: C, 64.20; H, 5.72; N, 14.04. Found: C, 64.24; H, 5.70; N, 14.02.

General procedure for the synthesis of compounds 29 and 33. K_2CO_3 (3.0 eq.) was added to a solution of azo compounds **26** and **28** (1.0 eq.) in an excess of dimethyl sulfate (3.0 mL). The blue/purple mixture was stirred at r.t. until completion of the reaction. Then, the reaction mixture was poured into water and extracted with DCM three times. The combined organic layers were dried over anhydrous Na_2SO_4, filtered, and evaporated *in vacuo*. Silica gel column chromatography allowed us to obtain the desired compound (eluent: *n*-hexane/ethyl acetate). These azo compounds were further purified by recrystallization from EtOH.

*(E)-1-(5-Isopropyl-4-methoxy-2-methylphenyl)-2-(4-methoxyphenyl)diazene (**29**).* Orange solid, m.p.: 64–66 °C, 76% yield. ^{1}H NMR (300 MHz, $CDCl_3$) δ 1.22 (d, J = 6.6 Hz, 6H, 2 iPr CH_3), 2.71 (s, 3H, Ar–CH_3), 3.26–3.31 (m, 1H, iPr CH), 3.89 (s, 3H, OCH_3), 3.90 (s, 3H, OCH_3), 6.76 (s, 1H, Ar), 7.00 (dt, J = 9.5, 2.6 Hz, 2H, Ar), 7.65 (s, 1H, Ar), 7.90 (dt, J = 9.6, 2.7 Hz, 2H, Ar). ^{13}C NMR (75 MHz, $CDCl_3$) δ 17.4, 22.6, 26.9, 55.5, 110.0, 112.06, 113.4, 114.1, 124.3, 135.4, 137.5, 144.5, 147.7, 159.1, 161.2. Anal. calcd for $C_{18}H_{22}N_2O_2$: C, 72.46; H, 7.43; N, 9.39. Found: C, 72.49; H, 7.45; N, 9.41.

*(E)-1-(5-Isopropyl-4-methoxy-2-methylphenyl)-2-(4-nitrophenyl)diazene (**33**).* Red solid, m.p.: 122–123 °C, 79% yield. ^{1}H NMR (300 MHz, $CDCl_3$) δ 1.25 (d, J = 6.6 Hz, 6H, 2 iPr CH_3), 2.75 (s, 3H, Ar–CH_3), 3.26–3.31 (m, 1H, iPr CH), 3.93 (s, 3H, OCH_3), 6.80 (s, 1H, Ar), 7.72 (s, 1H, Ar), 7.98 (dt, J = 9.3, 2.4 Hz, 2H, Ar), 8.36 (dt, J = 9.3, 2.4 Hz, 2H, Ar). ^{13}C NMR (75 MHz, $CDCl_3$) δ 17.5, 22.5, 26.8, 55.6, 112.1, 113.6, 123.1, 124.7, 135.9, 140.4, 144.6, 147.9, 156.6, 161.0. Anal. calcd for $C_{18}H_{22}N_2O_2$: C, 72.46; H, 7.43; N, 9.39. Found: C, 72.49; H, 7.41; N, 9.37.

General procedure for the synthesis of compounds 30 and 34. $NaHCO_3$ (3.0 eq.) was added to a solution of azo compounds **26** and **28** (1.0 eq.) in an excess of acetic anhydride (4.0 mL). The reaction mixture was stirred at r.t. till completion. Then, the reaction mixture was evaporated *in vacuo* to remove excess Ac_2O and the formed acetic acid, solubilized in DCM, and filtered to remove salts. No further purification was required. The compounds were further purified by recrystallization from EtOH.

*(E)-2-Isopropyl-4-((4-methoxyphenyl)diazenyl)-5-methylphenyl acetate (**30**).* Red solid, m.p.: 102–104 °C, 64% yield. Characterization data were in agreement with previous literature.[26] Anal. calcd for $C_{19}H_{22}N_2O_3$: C, 69.92; H, 6.79; N, 8.58. Found: C, 69.95; H, 6.77; N, 8.60.

*(E)-2-Isopropyl-5-methyl-4-((4-nitrophenyl)diazenyl)phenyl acetate (**34**).* Red solid, m.p.: 137–138 °C, 78% yield. Characterization data were in agreement with previous literature.[26] Anal. calcd for $C_{19}H_{22}N_2O_3$: C, 69.92; H, 6.79; N, 8.58. Found: C, 69.96; H, 6.81; N, 8.55.

General procedure for the synthesis of compounds 31, 32, 35, and 36. K_2CO_3 (1.5 eq.) was added to a solution of azo compounds **26** and **28** (1.0 eq.) and dimethyl (thio)carbamoyl chloride (1.8 eq.) in acetonitrile (0.4 M) at r.t. Once the reaction was completed, the reaction mixture was evaporated *in vacuo* to remove the excess reagents, solubilized in DCM, and filtered to remove the salts. Silica gel column chromatography allowed the obtainment of the desired compound (eluent: *n*-hexane/ethyl acetate). The compounds were further purified by recrystallization from EtOH.

*(E)-2-Isopropyl-4-((4-methoxyphenyl)diazenyl)-5-methylphenyl dimethylcarbamate (**31**).* Orange solid, m.p.: 90–92 °C. 64%

Open Access Article. Published on 09 October 2024. Downloaded on 10/27/2025 5:03:29 PM.
This article is licensed under a Creative Commons Attribution-NonCommercial 3.0 Unported Licence.

yield. ^{1}H NMR (300 MHz, $CDCl_3$) δ 1.26 (d, J = 6.6 Hz, 6H, 2 iPr CH_3), 2.65 (s, 3H, Ar–CH_3), 3.05 (s, 3H, NCH_3), 3.07–3.11 (m, 1H, iPr CH), 3.15 (s, 3H, NCH_3), 3.89 (s, 3H, OCH_3), 7.03 (m, 3H, Ar), 7.60 (s, 1H, Ar), 7.91 (d, J = 9.0 Hz, 2H, Ar). ^{13}C NMR (75 MHz, $CDCl_3$) δ 17.1, 22.9, 27.7, 36.5, 36.8, 55.6, 110.0, 113.5, 114.1, 124.7, 124.8, 136.4, 138.5, 147.5, 148.2, 150.5, 154.7, 161.7. Anal. calcd for $C_{19}H_{22}N_2O_3$: C, 67.58; H, 7.09; N, 11.82. Found: C, 67.62; H, 7.07; N, 11.80.

*(E)-O-(2-Isopropyl-4-((4-methoxyphenyl)diazenyl)-5-methylphenyl) dimethylcarbamothioate (**32**).* Orange solid, m.p.: 123–124 °C, 60% yield. ^{1}H NMR (300 MHz, $CDCl_3$) δ 1.26 (d, J = 7.2 Hz, 6H, 2 iPr CH_3), 2.62 (s, 3H, Ar–CH_3), 2.95–3.04 (m, 1H, iPr CH), 3.37 (s, 3H, NCH_3), 3.48 (s, 3H, NCH_3), 3.89 (s, 3H, OCH_3), 6.96 (s, 1H, Ar), 6.99 (d, J = 9.0 Hz, 2H, Ar), 7.64 (s, 1H, Ar), 7.91 (d, J = 9.0 Hz, 2H, Ar). ^{13}C NMR (75 MHz, $CDCl_3$) δ 17.2, 23.0, 27.5, 38.7, 43.3, 55.6, 113.7, 114.2, 124.7, 125.5, 136.3, 139.1, 147.4, 148.6, 152.9, 161.8, 187.5. Anal. calcd for $C_{20}H_{25}N_3O_2S$: C, 64.66; H, 6.78; N, 11.31. Found: C, 64.70; H, 6.80; N, 11.28.

*(E)-2-Isopropyl-5-methyl-4-((4-nitrophenyl)diazenyl)phenyl dimethylcarbamate (**35**).* Red solid, m.p.: 129–130 °C, 92% yield. ^{1}H NMR (300 MHz, $CDCl_3$) δ 1.27 (d, J = 6.9 Hz, 6H, 2 iPr CH_3), 2.71 (s, 3H, Ar–CH_3), 3.06 (s, 3H, NCH_3), 3.09–3.13 (m, 1H, iPr CH), 3.16 (s, 3H, NCH_3), 7.12 (s, 1H, Ar), 7.68 (s, 1H, Ar), 8.01 (dt, J = 11.6, 2.3 Hz, 2H, Ar), 8.40 (dt, J = 9.5, 2.3 Hz, 2H, Ar). ^{13}C NMR (75 MHz, $CDCl_3$) δ 17.1, 22.8, 27.57, 36.5, 36.8, 113.6, 123.4, 124.7, 125.2, 138.7, 139.0, 148.0, 148.4, 152.4, 154.4, 156.2. Anal. calcd for $C_{19}H_{22}N_2O_3$: C, 67.58; H, 7.09; N, 11.82. Found: C, 67.62; H, 7.11; N, 11.85.

*(E)-O-(2-Isopropyl-5-methyl-4-((4-nitrophenyl)diazenyl)phenyl) dimethylcarbamothioate (**36**).* Red solid, m.p.: 166–170 °C, 86% yield. ^{1}H NMR (300 MHz, $CDCl_3$) δ 1.27 (d, J = 6.9 Hz, 6H, 2 iPr CH_3), 2.72 (s, 3H, Ar–CH_3), 2.97–3.06 (m, 1H, iPr CH), 3.93 (s, 3H, NCH_3), 3.49 (s, 3H, NCH_3), 7.02 (s, 1H, Ar), 7.71 (s, 1H, Ar), 8.04 (d, J = 9.6 Hz, 2H, Ar), 8.37 (d, J = 9.6 Hz, 2H, Ar). ^{13}C NMR (75 MHz, $CDCl_3$) δ 17.2, 23.0, 23.6, 27.4, 37.1, 38.7, 43.3, 112.7, 113.8, 123.4, 123.6, 124.7, 126.1, 138.4, 139.6, 148.4, 148.4, 150.9, 154.6, 156.2, 187.1. Anal. calcd for $C_{20}H_{25}N_3O_2S$: C, 64.66; H, 6.78; N, 11.31. Found: C, 64.62; H, 6.76; N, 11.29.

4.2. Antibacterial activity evaluation

H. pylori strains were NCTC 11637 and clinical isolates F1, 23, and F4. The MIC determination was performed using a modified broth microdilution assay as previously described.[60] For MBC, 10 μL of suspensions without visible growth were spotted on the surface of Skirrow agar plates and incubated for 72 h at 37 °C under microaerophilic conditions and 100% humidity. The MBC was defined as the concentration that killed 99.9% of the initial inoculum. The MIC and MBC assessment was performed in triplicate, at least on three different days.

Escherichia coli ATCC 25922 was cultured on MacConkey agar (Oxoid) for 18 h at 37 °C, *Pseudomonas aeruginosa* ATCC 27853 on agar cetrimide for 18 h at 37 °C, and *Staphylococcus aureus* on mannitol salt agar (MSA) (Oxoid) for 24 h at 37 °C. MIC determination was performed on 96-well microtiter plates using a microdilution method in cation-adjusted Mueller Hinton broth (CAMHB).[61] All the plates were incubated at 37 °C for 24 h. After incubation, the lowest concentration of the compounds inhibiting visible growth was considered to be the MIC. For MBC, aliquots (10 μL) of suspensions without visible growth were plated on Mueller Hinton agar and incubated at 37 °C for 24 h. The MBC was defined as the lowest concentration of compounds that killed ≥99.9% of the initial inoculum.

4.3. *In silico* studies

Docking simulations. Molecular modelling studies were conducted using the Schrödinger Life-Sciences Suite 2024-1.[40] The ligands were drawn as 2D structures from Maestro and prepared using LigPrep to generate 3D geometry. All possible tautomers and protonation states at pH 7.0 ± 0.4 were identified using Epik.[62] The 3D structures of *Hp* urease and *Hp* FabZ were retrieved by Protein Data Bank (PDB ID 6ZJA and 3DOZ, respectively), while the 3D structure of *Hp*-G6PD and *Hp*-IMPDH were obtained through homology modelling. The primary sequences of *Hp*-G6PD (UniProt ID P56110, 425 aa) and *Hp*-IMPDH (Uniprot ID P56088, 481 aa) were retrieved from the UniProt KnowledgeBase database.[63] The protein sequences were utilized as a query sequence for homology modelling with Prime. The tool utilized BLAST[42] to align sequences and identify appropriate templates from the Protein Data Bank using a single template protocol. The homology model of *Hp*-G6PD was obtained using the structure of G6PD from *Leishmania donovani* G6PD (PDB ID 7ZHV, identity 31.74%) as the template, while *Hp*-IMPDH was modelled on the structure of IMPDH from *Cp* (PDB ID 4MZ1, identity 60.22%). The crystallographic coordinates of the IMP ligand complex with *Cp* (PDB ID 4MZ1)[45] were used to incorporate the ligand into the homology model of *Hp*-IMPDH. The protein–ligand complex was fully minimized using MacroModel and the OPLS4 force field. The residue positioning was optimized through 5000 steps of the PRCG minimization algorithm with a convergence criterion of 0.05 kJ mol^{-1} Å^{-1}. Molecular docking analyses were conducted using the Glide software. The Glide Grid was generated by placing the enclosing box at the center of mass of the ligand. The SP docking protocol was employed. In the initial phase, 5000 poses per ligand were specified, and 400 poses per ligand were set for energy minimization using the OPLS4 force field.

Physicochemical and pharmacokinetics properties calculations. ADME properties were calculated on the pkCSM web tool (**https://biosig.unimelb.edu.au/pkcsm/prediction**) that combines two main sets of descriptors to predict the physicochemical properties of the compounds: distance-based graphic signatures and the general properties of ligands.[47]

4.4. Cell-based assays

Cell cultures. Human gastric epithelial SV40-immortalized non-tumorigenic GES-1 cells (kindly provided by Prof. Dawid

Open Access Article. Published on 09 October 2024. Downloaded on 10/27/2025 5:03:29 PM.
This article is licensed under a Creative Commons Attribution-NonCommercial 3.0 Unported Licence.

Kidane, Department of Pharmacology and Toxicology, University of Texas, Austin, TX, USA) were cultured in RPMI medium (HyClone, Logan, UT, USA) supplemented with 10% decomplemented fetal calf serum (FCS) (HyClone), 1% levoglutamine (Sigma-Aldrich s.r.l., Milan, Italy), 1% pen/strep (HyClone), and 10 mM HEPES (Sigma-Aldrich). Human normal epithelial cells isolated from the small intestine (HIEC-6/CRL-3266) were purchased from ATCC and subcultured in complete DMEM/F12 medium supplemented with 4% inactivated fetal bovine serum (FBS), 1% penicillin/streptomycin, 20 mM HEPES, 10 mM glutamine (all from EuroClone, Milan, Italy) and 10 ng mL^{-1} of epidermal growth factor (EGF) (ThermoFisher Scientific, MA, USA). Cells were maintained in a 5% CO_2 atmosphere at 37 °C.

Cell viability assay (Alamar blue assay). Cell toxicity on GES-1 cells was determined using Alamar blue (AB) assay according to the manufacturer's instructions. Briefly, after the drug treatment at different time points (24 h, 48 h, 72 h), the AB reagent was added to each well. The plates were incubated at 37 °C for 4 h. Growth control (cells + broth + AB), medium control (only broth), and negative control (broth + AB), were also included. Growth was indicated by a change in color from dark blue to pink. The plates were then read on a microplate reader using the test wavelengths of 540 nm and 630 nm. The percent reduction of AB in the treated and untreated samples was calculated by using the formula indicated by the manufacturer.

MTT assay. The viability of HIEC-6 cells was measured using 3-(4,5-dimethylthiazol-2-yl)-2,5-diphenyltetrazolium bromide assay (MTT, Merck, Milan, Italy). After the exposure, cells were incubated with 100 μL per well MTT (5 mg mL^{-1}) diluted 1 : 10 with fresh growth medium for 4 h at 37 °C and 5% CO_2. Then, the MTT solution was removed to be replaced with 100 μL per well DMSO. Cells were further incubated for 20 min in the same conditions and gently swirled for 10 min at r.t. Absorbances were registered by means of a multiscan GO microplate spectrophotometer (Thermo Fisher Scientific, Waltham, MA, USA).

Data availability

This published article and its ESI† include all data generated or analyzed during this study.

Author contributions

Conceptualization, review and editing: S. C., I. D. A., A. A., F. S., and A. A.-S. Methodology and formal analysis: F. M., I. D. A., M. F., M. A., N. M., M. G., M. S., P. G., S. H. A, F. S., and S. C. Writing-original draft preparation: F. M., S. C., I. D. A., and P. G. All authors have read and agreed to the published version of the manuscript.

Conflicts of interest

The authors declare no conflict of interest.

Acknowledgements

This work was supported by FAR funding (Italian Ministry for Instruction, University, and Research) assigned to S. C. This article is based upon work from COST Action EURESTOP, CA21145, supported by COST (European Cooperation in Science and Technology) to S. C. and I. D. A. This publication was produced while attending the PhD programme in Biomolecular and Pharmaceutical Sciences at the University of Chieti-Pescara, Cycle XXXIX, with the support of a scholarship co-financed by the Ministerial Decree no. 117 of 02.03.2023, based on the NRRP - funded by the European Union - NextGenerationEU - Mission 4 "Education and Research", Component 2 "From Research to Business", Investment 3.3, and by the company IDI s.r.l. (N. M.).

References

1 A. Ali and K. I. AlHussaini, Helicobacter pylori: A Contemporary Perspective on Pathogenesis, Diagnosis and Treatment Strategies, *Microorganisms*, 2024, **12**(1), 222.
2 C. Lu, Y. Yu, L. Li, C. Yu and P. Xu, Systematic review of the relationship of Helicobacter pylori infection with geographical latitude, average annual temperature and average daily sunshine, *BMC Gastroenterol.*, 2018, **18**(1), 50.
3 Y. C. Chen, P. Malfertheiner, H. T. Yu, C. L. Kuo, Y. Y. Chang and F. T. Meng, *et al.*, Global Prevalence of Helicobacter pylori Infection and Incidence of Gastric Cancer Between 1980 and 2022, *Gastroenterology*, 2024, **166**(4), 605–619.
4 P. Malfertheiner, M. C. Camargo, E. El-Omar, J. M. Liou, R. Peek and C. Schulz, *et al.*, Helicobacter pylori infection, *Nat. Rev. Dis. Primers*, 2023, **9**(1), 1–24.
5 Schistosomes, liver flukes and Helicobacter pylori, *IARC Monogr Eval Carcinog Risks Hum.*, 1994, vol. 61, pp. 1–241.
6 T. Furuta, M. Yamade, T. Kagami, T. Uotani, T. Suzuki and T. Higuchi, *et al.*, Dual Therapy with Vonoprazan and Amoxicillin Is as Effective as Triple Therapy with Vonoprazan, Amoxicillin and Clarithromycin for Eradication of Helicobacter pylori, *Digestion*, 2020, **101**(6), 743–751.
7 L. Boyanova, P. Hadzhiyski, R. Gergova and R. Markovska, Evolution of Helicobacter pylori Resistance to Antibiotics: A Topic of Increasing Concern, *Antibiotics*, 2023, **12**(2), 332.
8 J. J. Lima, C. D. Thomas, J. Barbarino, Z. Desta, S. L. Van Driest and N. El Rouby, *et al.*, Clinical Pharmacogenetics Implementation Consortium (CPIC) Guideline for CYP2C19 and Proton Pump Inhibitor Dosing, *Clin. Pharmacol. Ther.*, 2021, **109**(6), 1417–1423.
9 G. Benito, I. D'Agostino, S. Carradori, M. Fantacuzzi, M. Agamennone and V. Puca, *et al.*, Erlotinib-containing benzenesulfonamides as anti-Helicobacter pylori agents through carbonic anhydrase inhibition, *Future Med. Chem.*, 2023, **15**(20), 1865–1883.
10 I. D'Agostino, C. Ardino, G. Poli, F. Sannio, M. Lucidi and F. Poggialini, *et al.*, Antibacterial alkylguanidino ureas: Molecular simplification approach, searching for membrane-based MoA, *Eur. J. Med. Chem.*, 2022, **231**, 114158.

 This journal is © The Royal Society of Chemistry 2025

Open Access Article. Published on 09 October 2024. Downloaded on 10/27/2025 5:03:29 PM.
This article is licensed under a Creative Commons Attribution-NonCommercial 3.0 Unported Licence.

11 C. Ardino, F. Sannio, G. Poli, S. Galati, E. Dreassi and L. Botta, *et al.*, An update on antibacterial AlkylGuanidino ureas: Design of new derivatives, synergism with colistin and data analysis of the whole library, *Eur. J. Med. Chem.*, 2024, 116362.
12 FDA, FDA Approves New Antibiotic for Three Different Uses [Internet], available from: https://www.fda.gov/news-events/press-announcements/fda-approves-new-antibiotic-three-different-uses.
13 D. M. Klug, F. I. M. Idiris, M. A. T. Blaskovich, F. von Delft, C. G. Dowson and C. Kirchhelle, *et al.*, There is no market for new antibiotics: this allows an open approach to research and development, *Wellcome Open Res.*, 2021, **6**, 146.
14 M. Di Martino, L. Sessa, M. Di Matteo, B. Panunzi, S. Piotto and S. Concilio, Azobenzene as Antimicrobial Molecules, *Molecules*, 2022, **27**(17), 5643.
15 T. Tahir, M. I. Shahzad, R. Tabassum, M. Rafiq, M. Ashfaq and M. Hassan, *et al.*, Diaryl azo derivatives as anti-diabetic and antimicrobial agents: synthesis, in vitro, kinetic and docking studies, *J. Enzyme Inhib. Med. Chem.*, 2021, **36**(1), 1508–1519.
16 A. M. Khedr, M. Gaber and E. H. Abd El-Zaher, Synthesis, Structural Characterization, and Antimicrobial Activities of Mn(II), Co(II), Ni(II), Cu(II) and Zn(II) Complexes of Triazole-based Azodyes, *Chin. J. Chem.*, 2011, **29**(6), 1124–1132.
17 S. Jangra, G. Purushothaman, K. Juvale, S. Ravi, A. Menon and V. Thiruvenkatam, *et al.*, Synthesis and In Vitro Enzymatic Studies of New 3-Aryldiazenyl Indoles as Promising Helicobacter pylori IMPDH Inhibitors, *Curr. Top. Med. Chem.*, 2019, **19**(5), 376–382.
18 K. T. Chung, G. E. Fulk and M. Egan, Reduction of azo dyes by intestinal anaerobes, *Appl. Environ. Microbiol.*, 1978, **35**(3), 558–562.
19 F. Sisto, S. Carradori, P. Guglielmi, C. B. Traversi, M. Spano and A. P. Sobolev, *et al.*, Synthesis and Biological Evaluation of Carvacrol-Based Derivatives as Dual Inhibitors of H. pylori Strains and AGS Cell Proliferation, *Pharmaceuticals*, 2020, **13**(11), 405.
20 F. Sisto, S. Carradori, P. Guglielmi, M. Spano, D. Secci and A. Granese, *et al.*, Synthesis and Evaluation of Thymol-Based Synthetic Derivatives as Dual-Action Inhibitors against Different Strains of H. pylori and AGS Cell Line, *Molecules*, 2021, **26**(7), 1829.
21 S. Carradori, A. Ammazzalorso, S. Niccolai, D. Tanini, I. D'Agostino and F. Melfi, *et al.*, Nature-Inspired Compounds: Synthesis and Antibacterial Susceptibility Testing of Eugenol Derivatives against H. pylori Strains, *Pharmaceuticals*, 2023, **16**(9), 1317.
22 C. Kantar and N. Baltaş, *Azo dyes containing eugenol and guaiacol, synthesis, antioxidant and enzyme inhibitory*, 2016.
23 C. Kantar, N. Baltaş and Ş. Alpay Karaoğlu, Some azo dyes containing eugenol and guaiacol, synthesis, antioxidant capacity, urease inhibitory properties and anti-helicobacter pylori activity, *Rev. Roum. Chim.*, 2018, **63**, 189–197.
24 C. Kantar, N. Baltaş, Ş. A. Karaoğlu and S. Şaşmaz, New Potential Monotherapeutic Candidates for Helicobacter pylori: Some Pyridinazo Compounds Having Both Urease Enzyme Inhibition and Anti-Helicobacter pylori Effectiveness, *Pharm. Chem. J.*, 2021, **55**(3), 246–252.
25 C. Kantar, N. Baltaş, Ş. A. Karaoğlu and S. Şaşmaz, Some Schiff Bases Containing Eugenol and Guaiacol: Comparison of Urease Inhibition and Anti-Helicobacter pylori Activities with Its Azo Analogs, *Pharm. Chem. J.*, 2024, **57**(11), 1738–1744.
26 S. Moffa, S. Carradori, F. Melfi, A. Fontana, M. Ciulla and P. Di Profio, *et al.*, Fine-tuning of membrane permeability by reversible photoisomerization of aryl-azo derivatives of thymol embedded in lipid nanoparticles, *Colloids Surf., B*, 2024, **241**, 114043.
27 S. Galati, M. Di Stefano, E. Martinelli, G. Poli and T. Tuccinardi, Recent Advances in In Silico Target Fishing, *Molecules*, 2021, **26**(17), 5124.
28 R. Amoroso, L. De Lellis, R. Florio, N. Moreno, M. Agamennone and B. De Filippis, *et al.*, Benzothiazole Derivatives Endowed with Antiproliferative Activity in Paraganglioma and Pancreatic Cancer Cells: Structure-Activity Relationship Studies and Target Prediction Analysis, *Pharmaceuticals*, 2022, **15**(8), 937.
29 A. Daina, O. Michielin and V. Zoete, SwissTargetPrediction: updated data and new features for efficient prediction of protein targets of small molecules, *Nucleic Acids Res.*, 2019, **47**(W1), W357–W364.
30 F. Ciriaco, N. Gambacorta, D. Trisciuzzi and O. Nicolotti, PLATO: A Predictive Drug Discovery Web Platform for Efficient Target Fishing and Bioactivity Profiling of Small Molecules, *Int. J. Mol. Sci.*, 2022, **23**(9), 5245.
31 J. Nickel, B. O. Gohlke, J. Erehman, P. Banerjee, W. W. Rong and A. Goede, *et al.*, SuperPred: update on drug classification and target prediction, *Nucleic Acids Res.*, 2014, **42**(Web Server issue), W26–W31.
32 M. Awale and J. L. Reymond, Polypharmacology Browser PPB2: Target Prediction Combining Nearest Neighbors with Machine Learning, *J. Chem. Inf. Model.*, 2019, **59**(1), 10–17.
33 M. J. Keiser, B. L. Roth, B. N. Armbruster, P. Ernsberger, J. J. Irwin and B. K. Shoichet, Relating protein pharmacology by ligand chemistry, *Nat. Biotechnol.*, 2007, **25**(2), 197–206.
34 I. D'Agostino and C. S. Urease, in *Metalloenzymes: From Bench to Bedside*, ed. C. T. Supuran and W. A. Donald, 2023, pp. 393–410.
35 C. Li, P. Huang, K. Wong, Y. Xu, L. Tan, H. Chen, Q. Lu, C. Luo, C. Tam, L. Zhu, Z. Su and J. Xie, Coptisine-induced inhibition of Helicobacter pylori: elucidation of specific mechanisms by probing urease active site and its maturation process, *J. Enzyme Inhib. Med. Chem.*, 2018, **33**(1), 1362–1375.
36 E. S. Cunha, X. Chen, M. Sanz-Gaitero, D. J. Mills and H. Luecke, Cryo-EM structure of Helicobacter pylori urease with an inhibitor in the active site at 2.0 Å resolution, *Nat. Commun.*, 2021, **12**(1), 230.
37 W. Liu, C. Luo, C. Han, S. Peng, Y. Yang and J. Yue, *et al.*, A new beta-hydroxyacyl-acyl carrier protein dehydratase (FabZ) from Helicobacter pylori: Molecular cloning, enzymatic characterization, and structural modeling, *Biochem. Biophys. Res. Commun.*, 2005, **333**(4), 1078–1086.
38 L. He, L. Zhang, X. Liu, X. Li, M. Zheng and H. Li, *et al.*, Discovering Potent Inhibitors Against the β-Hydroxyacyl-Acyl Carrier Protein Dehydratase (FabZ) of Helicobacter pylori:

Open Access Article. Published on 09 October 2024. Downloaded on 10/27/2025 5:03:29 PM.
This article is licensed under a Creative Commons Attribution-NonCommercial 3.0 Unported Licence.

Structure-Based Design, Synthesis, Bioassay, and Crystal Structure Determination, *J. Med. Chem.*, 2009, **52**(8), 2465–2481.

39 B. Hernández-Ochoa, G. Navarrete-Vázquez, R. Aguayo-Ortiz, P. Ortiz-Ramírez, L. Morales-Luna, V. Martínez-Rosas, A. González-Valdez, F. Gómez-Chávez, S. Enríquez-Flores, C. Wong-Baeza, I. Baeza-Ramírez, V. Pérez de la Cruz and S. Gómez-Manzo, Identification and In Silico Characterization of Novel Helicobacter pylori Glucose-6-Phosphate Dehydrogenase Inhibitors, *Molecules*, 2021, **26**(16), 4955.

40 *Schrödinger Release 2024-1, Maestro, Glide, Protein Preparation Wizard, Epik, MacroModel, Prime*, Schrödinger, LLC, New York (NY), 2024.

41 H. M. Berman, T. Battistuz, T. N. Bhat, W. F. Bluhm, P. E. Bourne and K. Burkhardt, *et al.*, The Protein Data Bank, *Acta Crystallogr., Sect. D: Biol. Crystallogr.*, 2002, **58**(Pt 6 1), 899–907.

42 C. Camacho, G. Coulouris, V. Avagyan, N. Ma, J. Papadopoulos and K. Bealer, *et al.*, BLAST+: architecture and applications, *BMC Bioinf.*, 2009, **10**(1), 421.

43 I. Berneburg, S. Rahlfs, K. Becker and K. Fritz-Wolf, Crystal structure of Leishmania donovani glucose 6-phosphate dehydrogenase reveals a unique N-terminal domain, *Commun. Biol.*, 2022, **5**(1), 1–14.

44 R. Zhang, G. Evans, F. Rotella, E. Westbrook, E. Huberman and A. Joachimiak, *et al.*, Differential signatures of bacterial and mammalian IMP dehydrogenase enzymes, *Curr. Med. Chem.*, 1999, **6**(7), 537–543.

45 RCSB Protein Data Bank, RCSB PDB - 4MZ1: Crystal Structure of the Inosine 5′-monophosphate Dehydrogenase, with a Internal Deletion of CBS Domain from Campylobacter jejuni complexed with inhibitor compound P12 [Internet], available from: **https://www.rcsb.org/structure/4mz1**.

46 K. Juvale, G. Purushothaman, V. Singh, A. Shaik, S. Ravi and V. Thiruvenkatam, *et al.*, Identification of selective inhibitors of Helicobacter pylori IMPDH as a targeted therapy for the infection, *Sci. Rep.*, 2019, **9**(1), 190.

47 D. E. V. Pires, T. L. Blundell and D. B. Ascher, pkCSM: Predicting Small-Molecule Pharmacokinetic and Toxicity Properties Using Graph-Based Signatures, *J. Med. Chem.*, 2015, **58**(9), 4066–4072.

48 B. H. Jin, B. W. Yoo, J. Park, J. H. Kim, J. Y. Lee and J. S. Shin, *et al.*, Pharmacokinetic drug interaction and safety after coadministration of clarithromycin, amoxicillin, and ilaprazole: a randomised, open-label, one-way crossover, two parallel sequences study, *Eur. J. Clin. Pharmacol.*, 2018, **74**(9), 1149–1157.

49 L. Chen, Y. Gao, L. Zhu, H. Song, L. Zhao and A. Liu, *et al.*, Establishment and characterization of a GES-1 human gastric epithelial cell line stably expressing miR-23a, *Oncol. Lett.*, 2018, **16**(1), 977–983.

50 A. Fedi, C. Vitale, G. Ponschin, S. Ayehunie, M. Fato and S. Scaglione, In vitro models replicating the human intestinal epithelium for absorption and metabolism studies: A systematic review, *J. Control. Release*, 2021, **335**, 247–268.

51 C. Ardino, F. Sannio, C. Pasero, L. Botta, E. Dreassi and J. D. Docquier, *et al.*, The impact of counterions in biological activity: case study of antibacterial alkylguanidino ureas, *Mol. Diversity*, 2023, **27**(3), 1489–1499.

52 I. D'Agostino, G. E. Mathew, P. Angelini, R. Venanzoni, G. Angeles Flores and A. Angeli, *et al.*, Biological investigation of N-methyl thiosemicarbazones as antimicrobial agents and bacterial carbonic anhydrases inhibitors, *J. Enzyme Inhib. Med. Chem.*, 2022, **37**(1), 986–993.

53 C. Zamperini, G. Maccari, D. Deodato, C. Pasero, I. D'Agostino and F. Orofino, *et al.*, Identification, synthesis and biological activity of alkyl-guanidine oligomers as potent antibacterial agents, *Sci. Rep.*, 2017, **7**(1), 8251.

54 C. Pasero, I. D'Agostino, F. De Luca, C. Zamperini, D. Deodato and G. I. Truglio, *et al.*, Alkyl-guanidine Compounds as Potent Broad-Spectrum Antibacterial Agents: Chemical Library Extension and Biological Characterization, *J. Med. Chem.*, 2018, **61**(20), 9162–9176.

55 V. Puca, G. Turacchio, B. Marinacci, C. T. Supuran, C. Capasso and P. Di Giovanni, *et al.*, Antimicrobial and Antibiofilm Activities of Carvacrol, Amoxicillin and Salicylhydroxamic Acid Alone and in Combination vs. Helicobacter pylori: Towards a New Multi-Targeted Therapy, *Int. J. Mol. Sci.*, 2023, **24**(5), 4455.

56 B. R. Pirgonde and M. A. Pujar, Reactions of dichlorobis(cyclopentadienyl)titanium(IV) with diazo compounds, *Acta Chim. Hung.*, 1989, **126**(2), 247–249.

57 P. Sagar Vijay Kumar, L. Suresh, T. Vinodkumar, R. BenjaramM and G. V. P. Chandramouli, Zirconium Doped Ceria Nanoparticles: An Efficient and Reusable Catalyst for a Green Multicomponent Synthesis of Novel Phenyldiazenyl–Chromene Derivatives Using Aqueous Medium, *ACS Sustainable Chem. Eng.*, 2016, **4**(4), 2376–2386.

58 M. Amaravathi, S. Kanakaraju and G. V. P. Chandramouli, Synthesis and Characterization of Azobenzene–Porphyrins, *J. Heterocyclic Chem.*, 2013, **50**(2), 268–271.

59 S. M. Koshti, J. P. Sonar, A. E. Sonawane, Y. A. Pawar, P. S. Nagle, P. P. Mahulikar and D. H. More, Synthesis of Azo Compounds Containing Thymol Moiety, *Indian J. Chem., Sect. B: Org. Chem. Incl. Med. Chem.*, 2008, **47**(2), 329–331.

60 F. Sisto, M. M. Scaltrito, G. Russello, A. Bonomi and F. Dubini, Antimicrobial susceptibility testing of Helicobacter pylori determined by microdilution method using a new medium, *Curr. Microbiol.*, 2009, **58**(6), 559–563.

61 Clinical and Laboratory Standard Institute (CLSI), *Development of In Vitro Susceptibility Testing Criteria and Quality Control Parameters: Approved Guideline*, Clinical and Laboratory Standard Institute, Wayne, PA, USA, 3rd edn, 2008, vol. 28.

62 J. C. Shelley, A. Cholleti, L. L. Frye, J. R. Greenwood, M. R. Timlin and M. Uchimaya, Epik: a software program for pK(a) prediction and protonation state generation for drug-like molecules, *J. Comput.-Aided Mol. Des.*, 2007, **21**(12), 681–691.

63 UniProt Consortium, UniProt: the Universal Protein Knowledgebase in 2023, *Nucleic Acids Res.*, 2023, **51**(D1), D523–D531.

 This journal is © The Royal Society of Chemistry 2025